PERGAMON

International Journal of Solids and Structures 38 (2001) 685–716

INTERNATIONAL JOURNAL OF SOLIDS and STRUCTURES

www.elsevier.com/locate/ijsolstr

Pulse scattering by a subsurface semi-infinite crack

R.V. Craster [a,*], D.P. Williams [b,1]

[a] *Department of Mathematics, Imperial College of Science, Technology and Medicine, London SW7 2BZ, UK*
[b] *Division of Theoretical Mechanics, School of Mathematical Sciences, University of Nottingham, Nottingham NG7 2RD, UK*

Received 8 September 1999; in revised form 20 March 2000

Abstract

Complementary techniques are used to investigate the dynamic loading of subsurface cracks in either homogeneous or non-homogeneous media; the quantities of interest such as the scattered fields and the stress intensity factors are determined. For homogeneous media, these involve solutions utilising transform methods and the Wiener–Hopf technique. To ease interpretation, an iterative method based on physical considerations is developed. For special loadings, invariant integrals are utilised to provide non-trivial extensions of the analysis to non-homogeneous media, at least insofar as the stress intensity factors are concerned.

Keywords: Fracture; Non-homogeneous media; Invariant integrals; Weight functions

1. Introduction

The dynamic stress loading of cracks, and the related fracture mechanics, is an area that has received much attention; for a detailed description see Freund (1990), Atkinson and Craster (1995b). There is particular interest in wave or pulse interactions with cracks that lie beneath surfaces or interfaces, as material failure or interfacial debonding is often caused by the subsequent growth of cracks. There has also been resurgent interest in the modelling of fracture in non-homogeneous solids (Craster and Atkinson, 1994; Choi, 1997; Ergüven and Gross, 1999), as modern fabrication methods and functionally graded materials become of more use; thus, we also address some aspects of crack-wave interactions in non-homogeneous media.

Determining the stress fields, and crack tip stress intensity factors, generated by the interaction of stress waves with cracks, and boundaries, is of fundamental interest in fracture mechanics. It is also of great interest in the non-destructive evaluation of structures. The scattered field yields information for crack detection and characterisation, thereby enabling estimates to be made of the location and size of the crack. The presence of an interface or free surface is a complicating feature and analytical solutions are often

* Corresponding author. Fax: +44-207-594-8517.
E-mail address: r.craster@ma.ic.ac.uk (R.V. Craster).
[1] Current address: Marine Physical Laboratory, Scripps Institution of Oceanography, University of California at San Diego, La Jolla CA 92093-0238, USA.

0020-7683/01/$ - see front matter
PII: S0020-7683(00)00109-8

difficult to obtain (Tsai and Ma, 1992, 1993). In these previous analyses for in-plane loadings the results are valid until the first wave scattered from the crack returns to the crack after having been reflected by the free surface. With the addition of an overlying fluid there are no current analyses. For anti-plane loadings the analysis becomes slightly simpler. One can utilise the method of images (Achenbach, 1973) for some rather special problems to extract the full solutions; however typically the situations are often somewhat more complicated.

The aim of this paper is to develop approaches that generate the stress intensity factors and give the exact form of the wavefronts, up to a specified time, generated by the dynamic loading of a semi-infinite subsurface crack. For ease of exposition we consider cracks that are parallel to the interface, the results may be generalised to look at cracks arbitrarily orientated to the interface; these results are not presented here. A variety of different stress loadings may be considered and here we consider the crack to be subjected to a prescribed stress loading on the crack faces and if required this could be chosen to be that induced by an incident pulse and hence identical to a scattering problem. Unfortunately it turns out that the plane strain problem cannot currently be solved conveniently and with this in mind we introduce an iterative (or *generalised* Wiener–Hopf) method in which successively the Cagniard–de Hoop (Flinn and Dix, 1962; de Hoop, 1960) and Wiener–Hopf (Noble, 1958) techniques are applied to solve a matrix Wiener–Hopf equation. This follows the scheme presented by Haak and Kooij (1996) and Kooij and Quak (1988) for anti-plane problems. The application of the Cagniard–de Hoop technique follows Garvin (1956) and Harris (1980). The iterative scheme is illustrated in detail on an anti-plane crack problem and, in addition, we demonstrate how weight functions can be incorporated into the iterative scheme.

The analysis is performed using Fourier and Laplace transforms in space and time respectively. The Laplace transform in time, t, and its inverse, are defined as

$$\overline{f}(p) = \int_0^\infty f(t)\mathrm{e}^{-pt}\,\mathrm{d}t, \qquad f(t) = \frac{1}{2\pi\mathrm{i}}\int_{c-\mathrm{i}\infty}^{c+\mathrm{i}\infty} \overline{f}(p)\mathrm{e}^{pt}\,\mathrm{d}p \quad \text{for } \mathrm{Re}\,(c) > 0, \tag{1.1}$$

where the Laplace transform variable is p. The Fourier transform in one spatial direction, x, and its inverse, are defined as

$$\widetilde{f}(s) = \int_{-\infty}^\infty f(x)\mathrm{e}^{\mathrm{i}sx}\,\mathrm{d}x, \qquad f(x) = \frac{1}{2\pi}\int_{-\infty}^\infty \widetilde{f}(s)\mathrm{e}^{-\mathrm{i}sx}\,\mathrm{d}s, \tag{1.2}$$

where s is the Fourier transform variable. We also utilise the Cagniard–de Hoop technique.

One of the most useful results found during any study of crack behaviour is the stress intensity factor; it is the stress intensity factor that characterises the near crack tip stress field. Here the results for the stress intensity factors are checked, and in some cases extended, using an invariant integral based on a pseudo energy momentum tensor (Atkinson, 1977; Atkinson and Craster, 1995a); which is a generalisation of the Eshelby (1951, 1970) energy momentum tensor. In particular, for a class of crack loadings, it enables us to investigate the effects of material inhomogeneity without any need for Wiener–Hopf analysis. This is motivated by the current interest in non-homogeneous or layered media.

For simplicity, we treat a simple spatial form of stress loading on the crack faces. We then demonstrate how weight functions (Bueckner, 1970) can be deduced within this iterative procedure and this allows us to generalise the stress intensity factor results to deal with any stress loading.

The plan for the following five sections of this article is as follows: first, in Section 2, we consider the anti-plane problem of a semi-infinite crack in a layered elastic material. The exact solution is found as an inverse integral using the Wiener–Hopf technique. This integral could then be evaluated numerically; these results are not included. Instead, we employ an iterative *generalised* Wiener–Hopf method (Thau and Lu, 1971) that yields a series solution. The motivation for developing this approach is that the exact solution contains a triple integral to evaluate and this obscures the physical interpretation of the solution. Also, the analogous problem of a subsurface crack in an elastic solid cannot currently be solved conveniently as one

obtains a matrix Wiener–Hopf equation whose factorisation is awkward; we briefly consider this case in Section 5 for the special case of a spatially uniform crack loading. An invariant integral is introduced in Section 3 which is then used to explore some model non-homogeneous materials, the aim is to illustrate the method as a useful analytical tool. Following this, in Section 4, we develop an iterative weight function method thus enabling us to use the generalised ray method to find formulae for the stress intensity factors exact up to a specified time.

The in-plane crack problems are substantially more complicated, involving mode coupling at both the crack tip and the interfaces. We briefly illustrate how the techniques developed in the simpler anti-plane case carry across to this harder situation in Section 5. Finally, a summary of the results is given in Section 6.

2. Anti-plane loading

We consider an elastic layer in $0 < y < b$, bonded to a semi-infinite elastic material that occupies the half space $b < y < \infty$; along the interface, $y = b$, the stress and displacement fields of the two materials satisfy continuity conditions. Within the elastic layer, a semi-infinite crack is present along $y = a$ $(a < b)$ for $x > 0$; this is shown in Fig. 1. This figure also shows the first reflected waves for $t < r_1 + 2a/c$, where $r_1^2 = x^2 + (y-a)^2$; $b - a > 2a$. This is after the wave from the crack that has been reflected from the surface strikes the crack, but before this wave returns to the surface, and before the wave reflected by the interface strikes the crack.

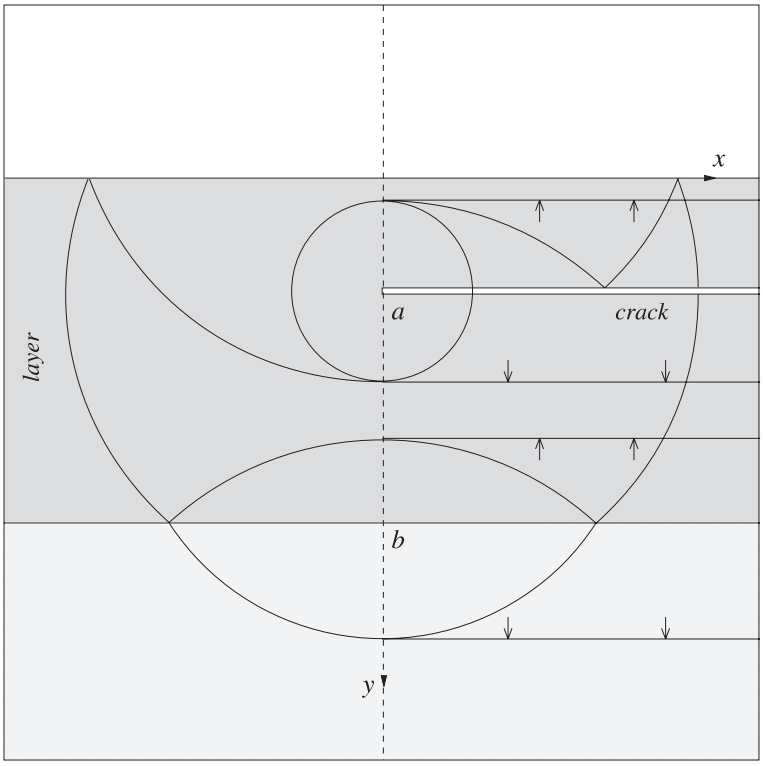

Fig. 1. The geometry of the problem shown together with a schematic of the first reflected waves.

A Cartesian coordinate system is adopted with x_1, x_2 corresponding to x and y. The problem is two-dimensional and the relevant stress components, $\sigma_{zj}(x,y,t)$, are related to the out-of-plane, that is, in the z direction displacements $u_z(x,y,t)$ via

$$\sigma_{zj} = \mu u_{z,j}, \tag{2.1}$$

where the comma denotes differentiation with respect to x_j and $\mu(x,y)$ is the elastic shear modulus. The governing equations are the equilibrium equations $\sigma_{zj,j} = \rho \ddot{u}_z$, where the notation denotes partial double differentiation with respect to time and $\rho(x,y)$ is the material density. The displacement satisfies

$$\left[\frac{\partial}{\partial x}\left(\mu\frac{\partial}{\partial x}\right) + \frac{\partial}{\partial y}\left(\mu\frac{\partial}{\partial y}\right)\right] u_z = \rho\ddot{u}_z \tag{2.2}$$

which reduces to the wave equation $\nabla^2 u_z = \ddot{u}_z/c^2$ when the material parameters μ and ρ are constant; the wavespeed c is then defined as $c^2 = \mu/\rho$. To distinguish between the different materials in the layer and underlying half space a superscript (h) is adopted to denote the elastic half space $y > b$. In this section, we henceforth assume that the material is homogeneous so μ and ρ are constant; we consider non-homogeneous materials in Section 3.

The surface $y = 0$ is taken to be rigid, hence, $u_z = 0$ there; a very similar analysis can be performed if the surface is stress-free. The crack lies in undamaged material so the condition taken ahead of the crack, $y = a$ for $x < 0$, is that the displacement u_z is continuous there, and the stress σ_{zy} is continuous along $y = a$, $-\infty < x < \infty$. The loading taken on the crack $y = a$, $x > 0$ is that $\sigma_{zy} = F(t)H(x)$, where $F(t)$ is the time dependence of the pulse and $H(x)$ is the Heaviside function. Later, in Section 4, we utilise our solution in conjunction with weight functions to extend our final results to any spatial loading. Along the interface, $y = b$, both the displacement u_z and stress σ_{zy} are continuous, i.e. $u_z = u_z^{(h)}$ and $\sigma_{zy} = \sigma_{zy}^{(h)}$.

2.1. Exact solution

First we shall solve the problem exactly, and then using an iterative approach. To formulate a functional equation, we apply Fourier transforms in the spatial x coordinate and Laplace transforms in time, together with the following half-range Fourier transforms: the transform of the unknown stress σ_{zy} ahead of the crack $y = a$ for $x < 0$, and the transform of the unknown jump in the displacement, u_z, across $y = a$ for $x > 0$,

$$\sigma_-(\xi,p) = \int_{-\infty}^{0} \overline{\sigma}_{zy}(x,a,p)\mathrm{e}^{\mathrm{i}\xi x}\,\mathrm{d}x, \qquad U_+(\xi,p) = \int_0^{\infty} [\overline{u}_z(x,a^+,p) - \overline{u}_z(x,a^-,p)]\mathrm{e}^{\mathrm{i}\xi x}\,\mathrm{d}x. \tag{2.3}$$

The subscripts $+$ and $-$ denote functions analytic in the 'plus' and 'minus' regions of the complex ξ plane, respectively; specifically in $\mathrm{Im}(\xi) > 0$ and in $\mathrm{Im}(\xi) < \min(p/c, p/c^{(h)})$, respectively. In the following, we loosely refer to these regions as the 'upper' and 'lower' halves of the complex ξ plane. The superscripts $+$ $(-)$ for a^+ (a^-) denote the limit as we approach the crack faces $(y = a)$ from above (below).

The Wiener–Hopf technique generates a functional equation that connects the transforms of these unknown quantities. This equation is then disentangled to identify the unknowns, and hence it determines the full solution. Along the way we require, of course, to satisfy the edge conditions, that is in terms of polar coordinates (r,θ) based at the crack tip, the displacements are $\mathrm{O}(r^{1/2})$ and the stresses are $\mathrm{O}(r^{-1/2})$ at the crack tip. The functional equation emerges as

$$\mathscr{Q}(\xi,p)[\sigma_-(\xi,p) + \Upsilon_+(\xi,p)] = -\mu\gamma(\xi,p)U_+(\xi,p), \quad \text{where } \Upsilon_+ = \frac{\overline{F}(p)}{\mathrm{i}\xi_+}; \tag{2.4}$$

the function Υ_+ has been introduced for convenience. To incorporate the specific loading adopted here, i.e., the spatially constant stress loading we adopt the convention that the pole at zero is in the lower half of the

complex ξ plane; this is, it is a 'plus' function and we remind ourselves of this fact using the subscript $+$ upon ξ and Υ. In Eq. (2.4), $\overline{F}(p)$ is the Laplace transform of the time dependence of the stress loading, $F(t)$, and the function $\gamma(\xi,p)$ $(\gamma(\xi,p)^{(h)})$ is defined as $\gamma(\xi,p)=[\xi^2+p^2/c^2]^{1/2}$ $(\gamma^{(h)}(\xi,p)=[\xi^2+p^2/c^{(h)^2}]^{1/2})$. The branch cuts for these functions, in the complex ξ plane, are taken such that they run along the imaginary axis from $\pm \mathrm{i}p/c$ $(\pm \mathrm{i}p/c^{(h)})$ to $\pm \mathrm{i}\infty$.

A function $\mathscr{Q}(\xi,p)$ is introduced in Eq. (2.4), and is defined as

$$\mathscr{Q}(\xi,p)\cosh(\gamma a)=\frac{\mu^{(h)}\gamma^{(h)}\sinh(\gamma b)+\mu\gamma\cosh(\gamma b)}{\mu^{(h)}\gamma^{(h)}\cosh[\gamma(b-a)]+\mu\gamma\sinh[\gamma(b-a)]}, \tag{2.5}$$

where $\gamma\equiv\gamma(\xi,p)$ and $\gamma^{(h)}\equiv\gamma^{(h)}(\xi,p)$. This function captures all the essential physics of the wave reflections from the surface, crack faces and interface together with the waveguide nature of the geometry.

The next step in our Wiener–Hopf recipe involves separating the functional equation (2.4) into a piece that is analytic in the $+$ region, and a piece that is analytic in the $-$ region. These pieces have a common overlapping region in the ξ plane, and thus are equal to the same analytic function within this strip. Hence, by analytic continuation, both sides *must* equal a function that is analytic everywhere. This must remain true even as $|\xi|\to\infty$, and so (by Liouville's Theorem) this function is a polynomial in ξ. This allows us to find the unknown transforms analytically. This polynomial is determined by applying the known edge behaviour at the crack tip, i.e., the stresses are $\mathrm{O}(r^{-1/2})$ there.

In order to make the split into the standard Wiener–Hopf form the function $\mathscr{Q}(\xi,p)$ is split into a product of $\pm$ functions: $\mathscr{Q}(\xi,p)=\mathscr{Q}_+(\xi,p)\mathscr{Q}_-(\xi,p)$; a related splitting is described in Appendix B, here, it is ultimately most easily performed in terms of some quadratures. We also require the product split $\gamma(\xi,p)=\gamma_+(\xi,p)\gamma_-(\xi,p)$, where $\gamma_\pm(\xi,p)=[\xi\pm \mathrm{i}p/c]_\pm^{1/2}$.

We now rearrange the functional Eq. (2.4) so that the left- and right-hand sides are analytic in the upper and lower halves of the complex ξ plane respectively:

$$\mu\frac{\gamma_+(\xi,p)}{\mathscr{Q}_+(\xi,p)}U_+ +\Upsilon_+\frac{\mathscr{Q}_-(0,p)}{\gamma_-(0,p)}=-\frac{\mathscr{Q}_-(\xi,p)}{\gamma_-(\xi,p)}\sigma_- -\Upsilon_+\left[\frac{\mathscr{Q}_-(\xi,p)}{\gamma_-(\xi,p)}-\frac{\mathscr{Q}_-(0,p)}{\gamma_-(0,p)}\right]. \tag{2.6}$$

The regions of analyticity overlap on $0<\mathrm{Im}\,(\xi)<\min\,(p/c,p/c^{(h)})$; this is enough to invoke analytic continuation and to determine that both sides of the functional equation can be extended to the full complex ξ plane, and hence are equal to the same analytic function everywhere. Using the edge conditions (the stresses in the limit as $r\to 0$ are $\mathrm{O}(r^{-1/2})$), this function is determined to be zero.

One of the most immediate results that can be deduced from the functional equation is the behaviour of the stress near the tip of the crack. The limit as $|\xi|\to\infty$ in the transform space corresponds to the limit as $x\to 0$ in the physical domain. The stress ahead of the tip of the crack is $\sigma_-(\xi,p)$ from which

$$\overline{\sigma}_{zy}(x,a,p)\sim\overline{F}(p)\left(\frac{c\mathscr{Q}(0,p)}{2p\pi}\right)^{1/2}(-x)^{-1/2}\equiv\overline{K}_{\mathrm{III}}(p)(-2\pi x)^{-1/2}\quad\text{for } x<0. \tag{2.7}$$

To obtain this result, we have employed the inverse Fourier transform given in Appendix A and the result $\mathscr{Q}_-(\xi,p)\to 2^{1/2}$ as $|\xi|\to\infty$. The mode III Laplace transformed stress intensity factor $\overline{K}_{\mathrm{III}}(p)\equiv\overline{K}(p)$ is also defined by Eq. (2.7) and hence can be explicitly extracted; that result is also extracted using an invariant integral in Section 3. The full solution for the stresses in the elastic layer is identified from Eq. (2.6) as

$$\sigma_{zy}(x,y,p)=\frac{1}{2\pi\mathrm{i}}\int_{c-\mathrm{i}\infty}^{c+\mathrm{i}\infty}\frac{1}{2\pi}\int_{-\infty}^{\infty}\frac{\overline{F}(p)\gamma_-(\xi,p)\mathscr{Q}_-(0,p)\cosh(\gamma y)}{\mathrm{i}\xi_+\gamma_-(0,p)\mathscr{Q}_-(\xi,p)\cosh(\gamma a)}\mathrm{e}^{-\mathrm{i}\xi x}\,\mathrm{d}\xi\,\mathrm{e}^{pt}\,\mathrm{d}p \tag{2.8}$$

for $0<y<a$. A similar expression may be deduced in $a<y<b$; these results are not included here. So far, we have taken the stress loadings to be uniform along the crack faces, however, we may routinely generalise

this to any loading of the form $\sigma_{zy} = F(t)G(x)$. For ease of presentation, we restrict ourselves to the stress intensity factors. The stress ahead of the crack tip is now asymptotically

$$\overline{\sigma}_{zy}(x,a,p) \sim -\overline{F}(p)\frac{1}{(2\pi \mathrm{i})_{-}^{1/2}}\left(\frac{1}{2\pi \mathrm{i}}\int_{-\infty}^{\infty}\frac{\mathscr{Q}_{-}(\chi,p)\widetilde{G}(\chi)}{\gamma_{-}(\chi,p)}\,\mathrm{d}\chi\right)(-x)^{-1/2}H(-x), \tag{2.9}$$

where $\widetilde{G}(\chi)$ is the Fourier transform of $G(x)$ (with Fourier transform variable χ). We also note that $\mathscr{Q}_{-}(\chi,p) \sim 2^{1/2} + \mathrm{O}(\mathrm{e}^{-2\gamma(\chi,p)a})$ to deduce the solution for a single crack in an infinite homogeneous material. This general formula is useful in comparison with one obtained later using weight functions.

These formulae formally solve the canonical problem. A direct numerical evaluation of the integrals above can be performed, but this is not overly revealing. In case when we expect the first few arrivals to completely characterise the solution, it proves to be more straightforward to proceed iteratively. Hence we choose to develop a method that iteratively solves Eq. (2.4) rather than formally expand the integral in Eq. (2.8).

In this section we have made a direct product split $\mathscr{Q} = \mathscr{Q}_{+}\mathscr{Q}_{-}$. The essence of a generalised ray approach is rather than digest $\mathscr{Q}$ in its entirety, we swallow it as smaller more manageable portions, i.e.,

$$\frac{1}{\mathscr{Q}} \sim \frac{1}{2}\left[1 + \exp[-2\gamma a] + \left(\frac{\mu(h)\gamma^{(h)} - \mu\gamma}{\mu(h)\gamma^{(h)} + \mu\gamma}\right)\exp[-2\gamma(b-a)] + \cdots\right] \tag{2.10}$$

and each term of $\mathscr{Q}$ now contains all the physics up to a specific time; the terms involving $\mu^{(h)}$, $\gamma^{(h)}$, μ, and γ can be identified with reflection coefficients from the interface or surface, and thus each term has physical significance. Each term of $\mathscr{Q}$ is ultimately split into a product $Q_{+}^{j}Q_{-}^{j}$ of $+$ and $-$ functions; however, the 'sum of products' that we construct does not, as a whole, have an obvious factorisation into a product of $+$ and $-$ functions so that $\mathscr{Q}_{+}$ (or $\mathscr{Q}_{-}$) is not easily recovered from its smaller portions as we may, at first, expect.

2.2. Iterative solution

In this section, we utilise an iterative scheme similar to that described by Kooij and Quak (1988) and Haak and Kooij (1996) to solve the problem we formulated in the previous section. This places the physical language of various superpositions, see for instance Tsai and Ma (1993), in a more rigorous setting. This approach lends itself well to further generalisations.

To formulate the current problem the original functional Eq. (2.4) is split into a series of less complicated subsidiary equations. Each equation then corresponds to the wavefield due to successive reflections from the crack, the interface and the surface. In the following, we drop the tilde and overline decoration on u_z and write $\widetilde{\overline{u}}_z(\xi,y,p)$ as u_z to shorten the notation; the same convention applies to σ_{zy}.

We expand u_z in generalised wave constituents, that is, each constituent has the property that its wavefront corresponds to the ray path that is described by a generalised ray of the same class (in the sense of number of reflections);

$$u_z = \sum_{m=0}^{\infty}\sum_{n=0}^{\infty} u_z^{(m,n)} \quad \text{in } 0 < y < a, \tag{2.11}$$

with a similar expression for u_z in $y > b$ and for σ_{zy}. Similarly we expand the unknown quantities in the transform domain $\sigma_{-} \equiv \sigma_{-}(\xi,p)$ and $U_{+} \equiv U_{+}(\xi,p)$; the arguments ξ and p are again omitted here and in $\gamma(\xi,p)$. The superscripts (m,n) correspond to m reflections against the interface, $y = b$, and the crack, and n reflections against the surface of the elastic layer, $y = 0$, and the crack. The functional Eq. (2.4) is rewritten as

$$2(\sigma_- + \Upsilon_+)\left(\frac{1+\mathscr{R}\mathrm{e}^{-2\gamma b}}{1-\mathscr{R}\mathrm{e}^{-2\gamma(b-a)}}\right) = -\mu\gamma\left(1+\mathrm{e}^{-2\gamma a}\right)U_+, \tag{2.12}$$

where $\mathscr{R}$ is the reflection coefficient at the interface of two dissimilar half spaces:

$$\mathscr{R} = \frac{\mu\gamma - \mu^{(h)}\gamma^{(h)}}{\mu^{(h)}\gamma^{(h)} + \mu\gamma}. \tag{2.13}$$

The reflection coefficient at a rigid surface is, of course, -1; so there is no need to introduce any extra notation for that reflection coefficient, although one can envisage having yet another elastic material in $y < 0$ and then requiring a reflection coefficient for reflected waves from $y = 0$. Using the expansion in Eq. (2.11), we split the functional equation (2.12) into a series of simple functional equations each of which is order $\exp[-2m\gamma(b-a) - 2n\gamma a]$. Doing so, we arrive at the following explicit functional equations:

$$\begin{aligned}
&s_-^{(0,0)} = -\tfrac{1}{2}\mu\gamma U_+^{(0,0)},\\
&s_-^{(0,n)} = -\tfrac{1}{2}\mu\gamma\left(U_+^{(0,n)} + U_+^{(0,n-1)}\mathrm{e}^{-2\gamma a}\right) \quad \text{for } n \geqslant 1,\\
&s_-^{(m,0)} + \sum_{q=0}^{m-1}\mathscr{R}^{m-q}\mathrm{e}^{-2(m-q)\gamma(b-a)}s_-^{(q,0)} = -\frac{1}{2}\mu\gamma U_+^{(m,0)} \quad \text{for } m \geqslant 1,\\
&s_-^{(m,n)} + \sum_{q=0}^{m-1}\mathscr{R}^{m-q}\left(s_-^{(q,n)} + \sigma_-^{(q,n-1)}\mathrm{e}^{-2\gamma a}\right)\mathrm{e}^{-2(m-q)\gamma(b-a)} = -\frac{1}{2}\mu\gamma\left(U_+^{(m,n)} + U_+^{(m,n-1)}\mathrm{e}^{-2\gamma a}\right) \quad \text{for } m,n \geqslant 1.
\end{aligned} \tag{2.14}$$

In these formulae $s_-^{(0,0)} = \sigma_-^{(0,0)} + \Upsilon_+$ and otherwise $s_-^{(m,n)} = \sigma_-^{(m,n)}$. To recover the stresses in $0 < y < a$, we require a further expansion that has the following form:

$$\sigma_{zy}^{(m,n)} = \left[\sum_{q=0}^{n}(-1)^q s_-^{(m,n-q)}\mathrm{e}^{-2q\gamma a}\right]\mathrm{e}^{-\gamma a}(\mathrm{e}^{\gamma y} + \mathrm{e}^{-\gamma y}); \tag{2.15}$$

recall that $\sigma_{zy} = \sum_{m=0}^{\infty}\sum_{n=0}^{\infty}\sigma_{zy}^{(m,n)}$. The stresses in $a < y < b$ and $b < y$ are not included here, but may be found in a similar way. Note that each successive solution in Eq. (2.15) includes both forward and backward going waves to $+\infty$ and $-\infty$, respectively, i.e. both the waves diffracted by the crack and reflected by the fixed surface at $y = 0$ and the interface at $y = b$ are described by a single iteration. A more physical approach that we could choose to exploit relies on a superposition of three separate problems. This approach is briefly described in Section 2.3.

2.2.1. First loading

The zero order functional equation from the first equation of Eq. (2.14) is

$$2\left(\sigma_-^{(0,0)} + \Upsilon_+\right) = -\mu\gamma U_+^{(0,0)}. \tag{2.16}$$

This is equivalent to the standard infinite medium problem (Freund, 1990) as the crack is initially unaware of either the surface or interface, and the unknown transforms emerge as

$$U_+^{(0,0)} = -\frac{2\Upsilon_+}{\mu\gamma_+(\xi,p)\gamma_-(0,p)}, \qquad \sigma_-^{(0,0)} = \Upsilon_+\left[\frac{\gamma_-(\xi,p)}{\gamma_-(0,p)} - 1\right], \tag{2.17}$$

from which we may deduce the zero order diffracted stress field explicitly. A more striking result that falls out of the analysis is the behaviour at the tip of the crack; we can extract the leading behaviour (using inverse Fourier results from Appendix A) as

$$\sigma_{zy}^{(0,0)}(x,a,t) \sim L^{-1}\left[\overline{F}(p)\left(\frac{2c}{p}\right)^{1/2}(-2\pi x)^{-1/2}\right], \tag{2.18}$$

where L denotes the Laplace transform operator. This result verifies, in part, the near stress field evaluated in Eq. (2.7).

It is straightforward to find the zero order solution utilising the Cagniard–de Hoop method, a detailed description of the method may be found in Miklowitz (1978) and others. In this case, it transpires that we require two different inversion contours, chosen so that $cT = (\zeta^2+1)^{1/2}(a-y) + \mathrm{i}\zeta x$ and $cT = (\zeta^2+1)^{1/2}(a+y) + \mathrm{i}\zeta x$, for time T real and positive. This is equivalent to constructing a generalised ray path; the path describes the vertical distance travelled by each wave, the total horizontal distance, and the direction of propagation. This device places the inverse Fourier integral in the form of a Laplace transform; in further iterations, this is not enough and we are required to formulate further Cagniard paths. We now require the inverse Laplace transform of this integral and as a result the solution in real time is found immediately by inspection. The explicit solution, for a general time dependence, is

$$\begin{aligned}\sigma_{zy}^{(0,0)}(x,y,t) = \int_0^t F(t-\tau)\frac{1}{\pi}\Bigg[&H(\tau - r_1/c)\mathrm{Re}\left(\frac{\gamma_-(\zeta_1(\tau))}{\mathrm{i}\zeta_1(\tau)\gamma_-(0)}\frac{\mathrm{d}\zeta_1(\tau)}{\mathrm{d}\tau}\right)\\ &+ H(\tau - r_2/c)\mathrm{Re}\left(\frac{\gamma_-(\zeta_2(\tau))}{\mathrm{i}\zeta_2(\tau)\gamma_-(0)}\frac{\mathrm{d}\zeta_2(\tau)}{\mathrm{d}\tau}\right)\Bigg]\mathrm{d}\tau.\end{aligned} \tag{2.19}$$

In this formula, $r_{1,2}^2 = x^2 + (y \mp a)^2$. We have also added some further decoration on the Cagniard paths: $cT = \gamma(\zeta_{1,2}(T))(a \mp y) + \mathrm{i}\zeta_{1,2}(T)x$, and a rescaling $\gamma(\zeta) = [\zeta^2+1]^{1/2}$. This solution corresponds to the cylindrical wavefields in $x<0$ generated by the crack and subsequently reflected by the surface $y=0$. It is formally valid in the interval $0 < t < (r_1+2a)/c$. In addition, in $x>0$ waves parallel to the crack faces are generated and in this case are given, by a residue calculation, in the form $F(t-(a-y)/c) + F(t-(a+y)/c)$. In further iterations, it is necessary to formulate the integral in terms of 'plus' and 'minus' functions in $x<0$ and $x>0$ respectively as a result of shifting the integration path in the upper and lower halves of the complex ξ plane. In Eq. (2.19), this distinction is not necessary. This result is plotted in Fig. 2 for the case $F(t) = \delta(t)$.

2.2.2. Reloading by the surface

To proceed we utilise the zero order solution we have determined in Section 2.2.1 to reload the crack and find the waves diffracted by the crack in this case. The Wiener–Hopf equation of exponential order $\exp[-2\gamma a]$ is given by Eq. (2.14) as

$$2\sigma_-^{(0,1)} = -\mu\gamma\left(U_+^{(0,1)} + \mathrm{e}^{-2\gamma a}U_+^{(0,0)}\right). \tag{2.20}$$

In order to utilise the Wiener–Hopf equation, we define $Q^{(0,1)} = \mathrm{e}^{-2\gamma a}$ and this function is split into the sum of $\pm$ functions, i.e. $Q^{(0,1)} = Q_+^{(0,1)} + Q_-^{(0,1)}$, where

$$Q_\pm^{(0,1)}(\xi,p) = \pm\frac{1}{2\pi\mathrm{i}}\int_{C_\pm}\frac{Q^{(0,1)}(\eta_1,p)}{\eta_1-\xi}\mathrm{d}\eta_1 = \pm\frac{1}{2\pi\mathrm{i}}\int_{C_\pm}\frac{\mathrm{e}^{-2\gamma(\eta_1,p)a}}{\eta_1-\xi}\mathrm{d}\eta_1, \tag{2.21}$$

and $Q_+^{(0,1)}(\xi,p) = Q_-^{(0,1)}(-\xi,p)$; C_+ (C_-) is the contour from $-\infty$ to ∞ indented below (above) the real axis. After some Wiener–Hopf analysis, we arrive at the following expressions for the unknown transforms:

$$\sigma_-^{(0,1)} = \frac{\gamma_-(\xi,p)\Upsilon_+}{\gamma_-(0,p)}\left[Q_-^{(0,1)}(\xi,p) - Q_-^{(0,1)}(0,p)\right], \qquad U_+^{(0,1)} = \frac{2\Upsilon_+\left[Q_+^{(0,1)}(\xi,p) + Q_-^{(0,1)}(0,p)\right]}{\mu\gamma_+(\xi,p)\gamma_-(0,p)}. \tag{2.22}$$

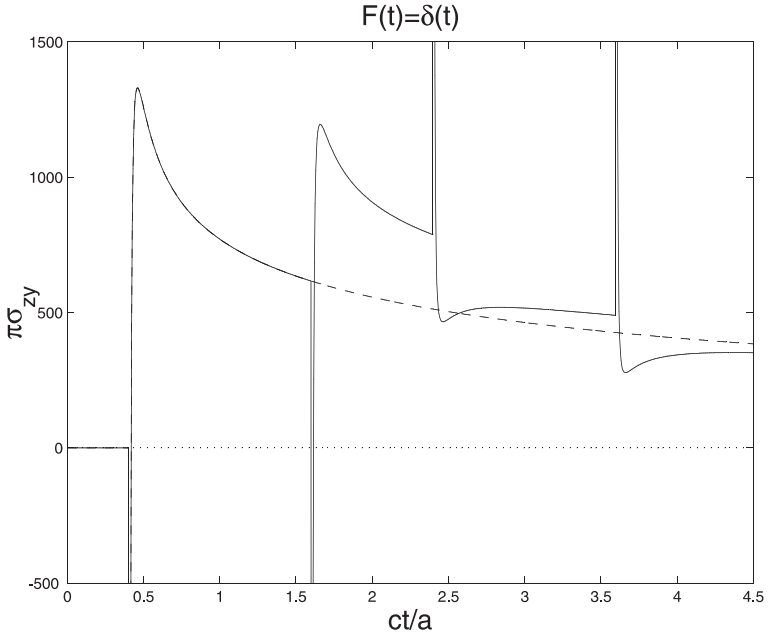

Fig. 2. The stress field for the case $F(t) = \delta(t)$ valid in $t < r_1 + 4a/c$ for $x/a = -0.02$ and $y/a = 0.6$; also shown by the $(\cdots)$ is the equivalent result in an infinite body.

2.2.2.1. Near crack tip stress field for $O(e^{-2\gamma a})$. We can again obtain the near tip behaviour either via taking the limit $|\xi| \to \infty$, that corresponds to $x \to 0$, in the inverse Fourier integral and evaluating the remaining integral in η_1, or equivalently utilising expression (2.22) directly. In the limit as $|\xi| \to \infty$ then $Q_+^{(0,1)}(\xi, p) \to 0$, and the near crack tip behaviour may now be extracted by evaluating $Q_-^{(0,1)}(0, p)$ only. This is obtained by collapsing the integral around the branch cut that runs from ip/c to $i\infty$ in the upper half plane and then evaluating the resulting definite integral using 3.7166 of Gradshteyn and Ryzhik (1980). That is

$$Q_-^{(0,1)}(0,p) = \frac{1}{\pi}\int_0^{\pi/2} \sin(2pa\tan\psi/c)\tan\psi \mathrm{d}\psi = \frac{1}{2}\mathrm{e}^{-2pa/c} = \frac{1}{2}Q^{(0,1)}(0,p), \tag{2.23}$$

so that we obtain

$$\sigma_{zy}^{(0,1)}(x,a,t) \sim -L^{-1}\left[\overline{F}(p)\left(\frac{2c}{p}\right)^{1/2}\frac{1}{2}\mathrm{e}^{-2ap/c}(-2\pi x)^{-1/2}\right]. \tag{2.24}$$

The results for the stress intensity factor presented here using an iterative approach are again consistent with those obtained by expanding Eq. (2.7). We provide a further check on this analysis using an invariant integral in Section 3.

2.2.2.2. Near crack tip stress field for $O(e^{-4\gamma a})$. Before we proceed to compute the stress field in this case, we briefly focus our attention on determining a further stress intensity factor. It is observed that the evaluation of further wavefields needs only the solution of a finite set of Wiener–Hopf equations. To evaluate this next reflection, we require

$$Q^{(0,2)}(\xi,p)=Q^{(0,1)}(\xi,p)\left[Q_+^{(0,1)}(\xi,p)+Q_-^{(0,1)}(0,p)\right]=Q_+^{(0,2)}(\xi,p)+Q_-^{(0,2)}(\xi,p), \tag{2.25}$$

where

$$Q_-^{(0,2)}(\xi,p)=-\frac{1}{2\pi\mathrm{i}}\int_{C_-}\frac{\mathrm{e}^{-2\gamma(\eta_2,p)a}}{\eta_2-\xi}\left[Q_+^{(0,1)}(\eta_2,p)+Q_-^{(0,1)}(0,p)\right]\mathrm{d}\eta_2, \tag{2.26}$$

and $Q_+^{(0,2)}(\xi,p)$ is similarly defined. As before, the near crack tip behaviour may now be extracted by evaluating $Q_-^{(0,2)}(0,p)=I_Q+\left[Q_-^{(0,1)}(0,p)\right]^2$. This is obtained by collapsing the integral I_Q around the branch cut that runs from $\mathrm{i}p/c$ to $\mathrm{i}\infty$ in the upper half plane, and in this case evaluating the resulting double definite integral:

$$I_Q=\frac{1}{\pi^2}\int_{p/c}^{\infty}\int_{p/c}^{\infty}\frac{\sin\left[2\left(\psi^2-\frac{p^2}{c^2}\right)^{1/2}a\right]\sin\left[2\left(\chi^2-\frac{p^2}{c^2}\right)^{1/2}a\right]}{\psi(\chi+\psi)}\mathrm{d}\chi\,\mathrm{d}\psi=\frac{1}{8}\mathrm{e}^{-4pa/c}. \tag{2.27}$$

Using this result, we have found $Q_+^{(0,2)}$ and hence the near crack tip behaviour:

$$\sigma_{zy}^{(0,2)}(x,a,t)\sim L^{-1}\left[\overline{F}(p)\left(\frac{2c}{p}\right)^{1/2}\frac{3}{8}\mathrm{e}^{-4ap/c}(-2\pi x)^{-1/2}\right]. \tag{2.28}$$

The stress intensity factors are discussed in detail in Section 3.

Following our short aside, the stress field may be written as

$$\sigma_{zy}^{(0,1)}(\xi,y,p)=-\overline{F}(p)\frac{\gamma_-(\xi,p)}{\gamma_-(0,p)}\left[\frac{1}{2\pi\mathrm{i}}\int_{-\infty}^{\infty}\frac{\mathrm{e}^{-2\gamma(\eta_1,p)a}}{\mathrm{i}\eta_1(\eta_1-\xi)}\mathrm{d}\eta_1\right]\left(\mathrm{e}^{\gamma(y-a)}+\mathrm{e}^{-\gamma(y+a)}\right), \tag{2.29}$$

where we have written $Q_+^{(0,1)}(\xi,p)$ and $Q_-^{(0,1)}(0,p)$ explicitly. In the present case, we wish to invert a transformed field quantity that already contains an integration over the variable η_1. Following Harris (1980), we introduce Cagniard contours in both the ζ plane, as described above, and the η_1 plane,

$$ct_1=2(\eta_1^2+1)^{1/2}a. \tag{2.30}$$

We shift the ζ and η_1 integrations onto contours along which T and t_1 are real. The η_1 path is defined by

$$\eta_1^{\pm}(t_1)=\pm\left[\left(\frac{ct_1}{2a}\right)^2-1\right]^{1/2}\quad\text{for }\frac{2a}{c}<t_1, \tag{2.31}$$

and the $\zeta_{1,2}(T)$ path employed in the first iteration is here expressed explicitly as

$$\zeta_{1,2}(T)=-\mathrm{i}\frac{cT}{r_{1,2}}\sin\theta_{1,2}+\left[\left(\frac{cT}{r_{1,2}}\right)^2-1\right]^{1/2}\cos\theta_{1,2}\quad\text{for }\frac{r_{1,2}}{c}<T; \tag{2.32}$$

we have taken the branch of the path with positive square root.

The modified Cagniard method (Harris, 1980) relies on a change of order of integration and the result $t=t_1+T$ to rewrite the integral in the usual Cagniard form. Then the time transform is of such a form that the inverse transform can be identified for any general loading, $F(t)$, in $0<y<a$ as

$$\begin{aligned}\sigma_{zy}^{(0,1)}(x,y,t)=\int_0^t F(t-\tau)\frac{1}{2\pi^2}\Bigg[&H(\tau-(r_1+2a)/c)\int_{r_1/c}^{\tau-2a/c}\mathscr{G}^{(0,1)}(\zeta_1(T),\eta_1(\tau-T))\,\mathrm{d}T\\&+H(\tau-(r_2+2a)/c)\int_{r_2/c}^{\tau-2a/c}\mathscr{G}^{(0,1)}(\zeta_2(T),\eta_1(\tau-T))\,\mathrm{d}T\Bigg]\mathrm{d}\tau,\end{aligned} \tag{2.33}$$

where the function $\mathscr{G}^{(0,1)}$ is defined by

$$\mathscr{G}^{(0,1)}(\zeta(T),\eta_1(t_1)) = -\mathrm{Im}\left[\frac{\partial\zeta}{\partial T}\frac{\gamma_-(\zeta)}{\gamma_-(0)}\left(\frac{1}{\mathrm{i}\eta_1^+(\eta_1^+-\zeta)}\frac{\partial\eta_1^+}{\partial t_1}-\frac{1}{\mathrm{i}\eta_1^-(\eta_1^--\zeta)}\frac{\partial\eta_1^-}{\partial t_1}\right)\right]. \tag{2.34}$$

In Fig. 2, the wavefield valid in time $0 < t < r_1 + 4a/c$, i.e. $\sigma_{zy} = \sigma_{zy}^{(0,0)} + \sigma_{zy}^{(0,1)} + \mathrm{O}(\mathrm{e}^{-6\gamma a}, \mathrm{e}^{-2\gamma(b-a)})$, until the second wave reflected by the surface returns to the crack, is shown in $x < 0$ and $0 < y < a$ for the loading $F(t) = \delta(t)$. In addition in $x > 0$ waves parallel to the crack faces are generated and proceed to be reflected by the surface in a similar way. There is a one-sided singularity associated with each cylindrical wavefront, and these can be seen in Fig. 2; further reflections give rise to other singularities.

As x/a is increased the sharp peak that occurs close to the wave arrival is smoothed out. When $y/a \ll 1$ and the observer is near to the fixed surface then the amplitude of the reflected wave is increased and arrives near to the wave incident on the surface. Similarly, when $y/a \sim 1$ and the observer is now near the crack then the diffracted wave and the wave incident on the crack arrive close together. These observations may be predicted by physical considerations.

So far the formulation and analysis has been for a crack in a semi-infinite half space $0 < y < \infty$; i.e. the crack is unaware that it is in a layer above a half space. In $0 < y < a$, the effect of the interface between the elastic layer and half space is first seen after time $t > r_1 + 2(b-a)/c$, i.e. after the first wave reflected by the interface returns to the crack. The previous analysis and Fig. 2 have assumed that $b - a > 2a$. This problem is considered briefly in Section 2.2.3.

2.2.3. Reloading by the interface

In this case, the Wiener–Hopf equation of exponential order $\exp[-2\gamma(b-a)]$ is given by Eq. (2.14) as

$$-2\left[\sigma_-^{(1,0)} + \mathscr{R}\left(\sigma_-^{(0,0)} + \Upsilon_+\right)\mathrm{e}^{-2\gamma(\xi,p)(b-a)}\right] = \mu\gamma U_+^{(1,0)}. \tag{2.35}$$

Following the approach used in Section 2.2.2, we define $Q^{(1,0)}(\xi,p) = \mathrm{e}^{-2\gamma(b-a)}$, split this into $\pm$ functions, $Q^{(1,0)} = Q_+^{(1,0)} + Q_-^{(1,0)}$, and extract the expressions for the unknown transforms:

$$\begin{aligned}
\sigma_-^{(1,0)} &= -\frac{\Upsilon_+\gamma_-(\xi,p)\mathscr{R}}{\gamma_-(0,p)}\left[Q_-^{(1,0)}(\xi,p) - Q_-^{(1,0)}(0,p)\right],\\
U_+^{(1,0)} &= -\frac{2\Upsilon_+\mathscr{R}\left[Q_+^{(1,0)}(\xi,p) + Q_-^{(1,0)}(0,p)\right]}{\mu\gamma_+(\xi,p)\gamma_-(0,p)}.
\end{aligned} \tag{2.36}$$

2.2.3.1. Near crack tip stress field for $O(e^{-2\gamma(b-a)})$. In the same way that we evaluated the near crack tip behaviour in Section 2.2.2 in this case it may be extracted by evaluating $Q_-^{(1,0)}(0,p)$. Again using integral 3.7166 in Gradshteyn and Ryzhik (1980) (or evenness of function $Q^{(1,0)}(\xi,p)$), we find that

$$\sigma_{zy}^{(1,0)}(x,a,t) \sim -L^{-1}\left[\overline{F}(p)\left(\frac{c}{p\pi}\right)^{1/2}\frac{1}{2}\Delta\mathrm{e}^{-2p(b-a)/c}(-x)^{-1/2}\right], \tag{2.37}$$

where $\Delta = (\mu c^{(h)} - \mu^{(h)}c)/(\mu^{(h)}c + \mu c^{(h)})$ and this result is consistent with the solution in Eq. (2.7).

Out of completeness, the stress field in this case is

$$\sigma_{zy}^{(1,0)}(\xi,y,p) = -\frac{\Upsilon_+\gamma_-(\xi,p)}{\gamma_-(0,p)}\mathscr{R}\left[Q_-^{(1,0)}(\xi,p) - Q_-^{(1,0)}(0,p)\right]\left(\mathrm{e}^{\gamma(y-a)} - \mathrm{e}^{-\gamma(y+a)}\right); \tag{2.38}$$

this expression may be routinely inverted using the Cagniard–de Hoop method described in Section 2.2.2.

2.3. Comment on fundamental solutions

An alternative approach of generating an iterative solution is to treat as separate problems the loading of the crack, the surface of the elastic layer, and the interface between the elastic layer and the underlying half space; each of these successive iterations takes the negative of the previous solution as its loading. This can be shown to be completely consistent with the analysis presented in the earlier sections and it has been used as a consistency check; the details are not included. Physically, this approach has some advantages over the iterative scheme used in Section 2.2 and in Haak and Kooij (1996); in a more complicated coupled situation, such as the in-plane scattering problem of Section 5, where identifying the wavefields is less elementary, it is sometimes more convenient to adopt this separation approach and extract each scattered field independently.

3. Invariant integral

In this section, attention is given to the field near the crack tip, which is completely characterised by the stress intensity factor, and in particular we focus upon non-homogeneous materials. The results for the near crack tip stresses for a homogeneous material have been presented in Sections 2.1 and 2.2; these results are also recovered using a path-independent integral. The basic method was first used in dynamic elasticity by Nilsson (1973). Following the approach initiated in elastostatics by Eshelby (1970), a Lagrangian is deduced in the Laplace transform domain in each material such that the Euler–Lagrange relations recover the governing equations; the Lagrangian L, is

$$L = -\tfrac{1}{2}\left(\overline{\sigma}_{zj}\overline{u}_{z,j} + \rho p^2 \overline{u}_z \overline{u}_z\right). \tag{3.1}$$

As this is defined in the transform domain this Lagrangian does not have the apparently obvious physical interpretation, i.e., one would hope it was the transform of the physical energy density. Unfortunately, the Lagrangian and pseudo energy momentum tensor involve products of Laplace transforms. The inverse transform of a product of transforms is not the product of the inverse transforms; which would lead to the obvious interpretation. But the inverse transform of a product is a convolution, hence, it is not clear what the physical meaning is. When we consider the layer-half space configuration of Section 2 this Lagrangian is defined in $0 < y < b$ and we also need to define a Lagrangian $L^{(h)}$ in $b < y$ by Eq. (3.1) with appropriate changes to material parameters. Initially, we treat a non-homogeneous half space and only need the first of these Lagrangians. The corresponding pseudo energy momentum tensor is

$$P_{lj} = \frac{\partial L}{\partial \overline{u}_{z,j}}\overline{u}_{z,l} - L\delta_{lj}; \tag{3.2}$$

again, unlike Eshelby's elastostatic energy momentum tensor the pseudo energy momentum tensor in the Laplace transform domain does not have any obvious physical interpretation. The Lagrangian does not depend explicitly on the space variable, and thus the integral, F_1, defined as

$$F_1 = \int_S P_{1j} n_j \,\mathrm{d}S \tag{3.3}$$

is zero provided that the path S does not enclose any singularities; n_j is the unit vector normal to S (Fig. 3). This integral is analogous to Rice's J integral (Rice, 1968) but is now also incorporating dynamic effects and the non-homogeneous material variation.

For anti-plane strain, the stress intensity factor can be rapidly evaluated using this invariant integral. Although it is important to realise that the technique only works neatly as a computational tool for spatially constant applied stress or displacement boundary conditions along the horizontal (x) boundaries and

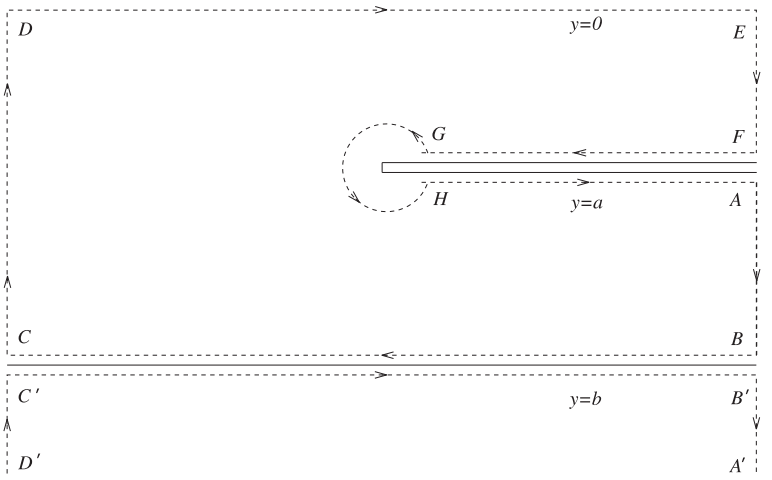

Fig. 3. The path, S, required for the application of the invariant integral in Section 3.

for material variation in the y coordinate. In the more complicated situations found for in-plane elastic problems mode coupling occurs at the crack tip and the method often leads to a representation for the sum of the squares of the stress intensity factors (Section 5). In static elasticity theory, this all reduces to the energy release rate, however we are currently in the Laplace transform domain, and it is unclear what physical significance, if any, these results have apart from neatly capturing the transformed stress intensity factors.

In essence, the information near to the crack tip can be obtained by studying the far away field; we evaluate the integrals far from the crack tip and relate this to the stress intensity factors. The behaviour near the tip of the crack is determined in terms of cylindrical polar coordinates (r,θ) centred on the tip with $\theta = 0$ ahead of the crack and the elastic material is in $-\pi \leqslant \theta \leqslant \pi$; the stress is locally $\overline{\sigma}_{zy} \sim \overline{K}(p)/(2\pi r)^{-1/2}\cos(\theta/2)$. The coefficient $\overline{K}(p)$, the stress intensity factor (in Laplace transform space), characterises the near tip singularity and here we shall extract it using the invariant integral. These near tip fields are used to evaluate the integral around GH (in path S).

To evaluate the stresses, we note that the derivatives with respect to x tend to zero as $x \to \pm\infty$. As a result, the governing equations become

$$\frac{\mathrm{d}\overline{\sigma}_{zy}}{\mathrm{d}y} = p^2\rho(y)\overline{u}_z, \quad \text{where } \overline{\sigma}_{zy} = \mu(y)\frac{\mathrm{d}\overline{u}_z}{\mathrm{d}y}. \tag{3.4}$$

When treating spatial variations in the shear modulus or density the application of the Wiener–Hopf method or numerical methods, to a semi-infinite crack problem, may be difficult. Currently much of the non-homogeneous fracture mechanics literature concentrates upon static situations, e.g. Ergüven and Gross (1999). However, the path independent integral is ideally suited to dealing with special situations (spatially constant loadings and material variation normal to the crack), and in fact the method gives results for any variation of modulus. Some related static problems are considered for general $\mu(y)$ in Atkinson and Craster (1995b).

For analytic simplicity, as in Atkinson (1975), we make the further restriction that the density ρ varies in such a way that $\rho(y)/\mu(y) = c^{-2}$ a constant. Introducing the substitution $v(y) = \mu^{1/2}(y)u_z(y)$ then enables the governing Eq. (3.4) to be rewritten as

$$\frac{\mathrm{d}^2 v}{\mathrm{d}y^2} = v\left[\frac{p^2}{c^2} + a(y)\right], \quad \text{where } a(y) = \frac{1}{4\mu}\left[2\frac{\mathrm{d}^2\mu}{\mathrm{d}y^2} - \frac{1}{\mu}\left(\frac{\mathrm{d}\mu}{\mathrm{d}y}\right)^2\right]. \tag{3.5}$$

We now make some specific choices for the material variation. The first choice, $\mu(y) = \alpha^2 \exp(2\beta y)$, where β, α are constant, has the advantage that the resulting function $a(y)$ is equal to β^2. This results in the simple solutions $v(y) = A\exp(-\Gamma y) + B\exp(\Gamma y)$, where $\Gamma = [(p/c)^2 + \beta^2]^{1/2}$, for constants A, B determined by the boundary conditions on $y = 0$ and $y = a$.

We now proceed to relate the integral around the crack tip to the known integrals around the body; the only integrals that contribute to the invariant are along EF, AB, (and $B'A'$ in an elastic layer), and the points at F and A along the crack faces. Performing the integrals we obtain

$$\overline{K}(p) = \overline{F}(p)\left[\frac{\Gamma(\sinh\Gamma a + \cosh\Gamma a)}{(\Gamma+\beta)(\Gamma\cosh\Gamma a - \beta\sinh\Gamma a)} + \frac{\beta}{2(\Gamma\cosh\Gamma a - \beta\sinh\Gamma a)^2}\right]^{1/2}. \tag{3.6}$$

It is perhaps surprising that the stress intensity factor is independent of the choice of α for this specific loading. A related choice of $\mu(y)$ in an infinite body is $\alpha^2\exp(2\beta|y-a|)$, which is a symmetric modulus variation about the fracture plane, in this case the Laplace transform of the stress intensity factor for an infinite body is

$$\overline{K}(p) = \overline{F}(p)\left(\frac{2}{\Gamma+\beta}\right)^{1/2}. \tag{3.7}$$

The stress intensity factors rescaled as $K(t)(\pi/8a)^{1/2}$ versus non-dimensional time ct/a are shown in Fig. 4; the Laplace transform (3.6) is inverted using an adaptation of the Fourier inversion routine described in Atkinson and Craster (1992a). The figure compares moduli variations; the second variation is described later. In panel (a) the modulus variations $\mu(y) = \alpha^2\exp(2\beta y)$ (—) and $\mu(y) = (\beta y + \alpha)^2$ $(\cdots)$ are shown for $\beta = 0.5/a$, $\alpha = 1$; the corresponding results for a crack in an infinite material are shown by $(- - -)$ and $(\cdots)$, respectively. For further comparison the dashed-dotted line $(- \cdot)$ shows the results for constant μ. The rather striking changes in the stress intensity factor in Fig. 4(a) are caused by the waves reflected from the surface reloading the crack; the reflections occur at equal values of ct/a since we have taken c to be constant. In panel (b), the effect of a modulus variation, symmetric about the fracture plane, on the intensity factor is shown for a crack in an infinite material with $\beta = 0.4/a$, $\alpha = 1$ and modulus variations $\mu(y) = \alpha^2\exp(2\beta|y-a|)$ (—) and $\mu(y) = (\beta|y-a| + \alpha)^2$ $(\cdots)$, and otherwise as in panel (a).

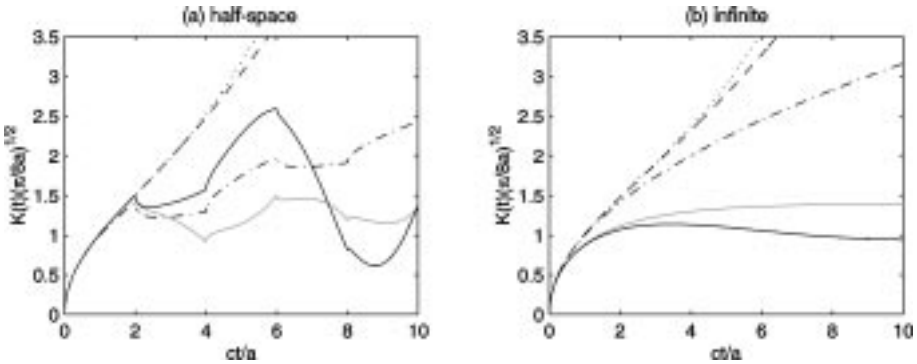

Fig. 4. Rescaled stress intensity factors for different moduli variations, see text for details.

Increasing the value of β in these results leads to larger peaks in the stress intensity factor as the material has decreasing rigidity in the layer between the crack and the surface; the net effect of which is to concentrate the wave energy near the surface and leads to a stronger reloading effect for waves reflected from the surface. The sharp reloadings become less evident, and this can already be partly seen in Fig. 4(a).

In contrast to Fig. 4(b), the symmetric modulus variation is crudely speaking analogous to a rigid boundary above and below the crack, we no longer obtain the sharp peaks due to the distinct reloadings caused by the reflections from a rigid boundary, but rather we get a continual and gradual reloading which causes the stress intensity factor to level off to a constant value $\beta^{-1/2}$.

To contrast with the earlier choice of an exponential variation we now choose a variation with algebraic growth, $\mu(y) = (\beta y + \alpha)^2$, which is also analytically rewarding. The stress intensity factor is shown in Fig. 4; the details of the figure have been given and are not repeated. This modulus variation leads to $a(y) = 0$ so that the solutions take the form $v(y) = A\sinh(py/c) + B\cosh(py/c)$. In general for $\mu(y) = (\beta y + \alpha)^n$ then $a(y) = n(n-2)\beta^2/4(\beta y + \alpha)^2$ and, therefore, in general we have to proceed numerically; this is not the case for $n = 2$. Evaluating the integrals and relating the non-zero contribution to the integral around the crack tip gives

$$\overline{K}(p) = \overline{F}(p)\left(\frac{p}{c}\right)^{1/2}\left[\frac{\sinh(pa/c) + \cosh(pa/c)}{\left(\frac{p}{c} + \frac{\beta}{(\beta a+\alpha)}\right)\left(\frac{p}{c}\cosh(pa/c) - \frac{\beta}{(\beta a+\alpha)}\sinh(pa/c)\right)}\right]^{1/2}. \tag{3.8}$$

A related result in an infinite material for a symmetric variation about the crack $\mu(y) = (\beta|y-a| + \alpha)^2$ is $\overline{K}(p) = \overline{F}(p)[2/(p/c + \beta/\alpha)]^{1/2}$. Under Heaviside loading $F(t) = H(t)$ this can be inverted to give an error function $K(t) = (2\alpha/\beta)^{1/2}\mathrm{erf}\sqrt{\beta ct/\alpha}$. A comparison between this result and the result in an infinite body is made in Fig. 4(b), the symmetric modulus variation which have increasing shear moduli as one moves away from the crack, have lower stress intensity factors as waves return to reload the crack from the regions with higher rigidity. In contrast to the symmetric exponential loading, the stress intensity factor approaches a constant value, $(2\alpha/\beta)^{1/2}$, monotonically from below.

These solutions provide useful benchmark examples upon which numerical solutions can be tested. In addition they demonstrate the effect of inhomogeneity can be to substantially amplify the stress intensity factors after successive reflections reload the crack. Note that when $\beta = 0$, in both the cases, we have considered in detail then the shear modulus is constant, $\mu = \alpha^2$, and we just recover the stress intensity factor for a cracked half space. For small β (or y) then for both cases, provided $\alpha = 1$, we find $\mu(y) \sim 1 + 2\beta y$ and we are in a position to compare algebraic and exponential variations and as we might expect the exponential growth leads to a stronger response with more noticeable peaks.

We now return to the layer-half space configuration of Sections 2.1 and 2.2, we can generalise the stress intensity factor results we have already obtained by using the invariant integral with a Lagrangian in the half-space and layer: For convenience, assume that both the layer and half space are homogeneous, then applying the invariant around the contour shown in Fig. 3 and evaluating the integrals along the sides of the strip, one deduces that

$$\overline{K}(p) = \overline{F}(p)\left(\frac{c}{p\cosh(pa/c)}\right)^{1/2}\left[\frac{\mu^{(h)}c\sinh(pb/c) + \mu c^{(h)}\cosh(pb/c)}{\mu^{(h)}c\cosh(p(b-a)/c) + \mu c^{(h)}\sinh(p(b-a)/c)}\right]^{1/2}. \tag{3.9}$$

Some representative numerical results are shown in Fig. 5(a) where we have chosen some typical values for the two free parameters b/a and $\mu c^{(h)}/\mu^{(h)}c$.

As an aside, the treatment of a layered-inhomogeneous material may, in certain considerations, be approximated by the suitably adjusted treatment of an n-layered material. The full solution of the n-layered problem is an arduous algebraic task since we are required to solve continuity conditions at each interface, however, the invariant integral yields the stress intensity factors very rapidly by utilising simplified

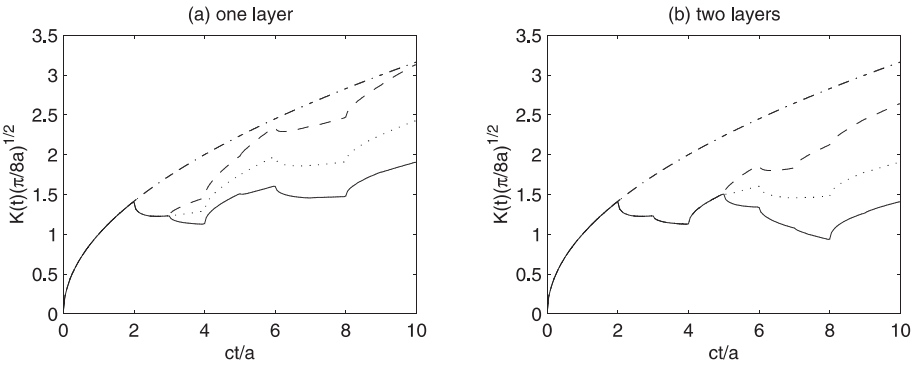

Fig. 5. Rescaled stress intensity factors for one or two layers above a half space; see text for details.

continuity conditions and only the integrals over the layers as $x \to \infty$. The following result is for two layers above a half space, but may be routinely extended to several layers. The elastic layer in $0 < y < b_1$ ($\equiv b$) is now labelled by a subscript 1, and the second elastic layer in $b_1 < y < b_2$ is denoted by 2; the half space is in $b_2 < y < \infty$,

$$\overline{K}(p) = \overline{F}(p)\left(\frac{c_1}{p\cosh(pa/c_1)}\right)^{1/2}\left[\frac{\mu_2 c_1\kappa_1\,\sinh(pb_1/c_1) + \mu_1 c_2\kappa_2\,\cosh(pb_1/c_1)}{\mu_2 c_1\kappa_1\,\cosh(p(b_1-a)/c_1) + \mu_1 c_2\kappa_2\,\sinh(p(b_1-a)/c_1)}\right]^{1/2}, \tag{3.10}$$

where $\bar{b} = b_2 - b_1$,

$$\kappa_1 = \frac{\mu_2}{c_2}\sinh\left(\frac{p\bar{b}}{c_2}\right) + \frac{\mu^{(h)}}{c^{(h)}}\cosh\left(\frac{p\bar{b}}{c_2}\right), \qquad \kappa_2 = \frac{\mu_2}{c_2}\cosh\left(\frac{p\bar{b}}{c_2}\right) + \frac{\mu^{(h)}}{c^{(h)}}\sinh\left(\frac{p\bar{b}}{c_2}\right). \tag{3.11}$$

In this case, we have five free parameters, b_1/a and $\mu_1 c^{(h)}/\mu^{(h)}c_1$, as before, and also b_2/a, c_1/c_2, and $\mu_1 c_2/\mu_2 c_1$.

The Laplace transforms (3.9) and (3.10) are again inverted numerically for the case $F(t) = H(t)$, and the stress intensity factors rescaled as $K(t)(\pi/8a)^{1/2}$ versus non-dimensional time ct/a are shown in Fig. 5. The rather striking changes in the stress intensity factor are, again, caused by the waves reflected from the surface, and this time also interface(s), reloading the crack. In Fig. 5(a) the solid and dashed lines show the stress intensity factor for positive and negative values of Δ (when $b - a > a$), respectively; either the waves in the layer travel faster than those in the half space (—) (the specific parameter values are that $b/a = 5/2$, $\mu = \mu^{(h)}$, and $c = 2c^{(h)}$) or the wavespeed in the layer is slower than that of the half space (– – –) ($\mu = \mu^{(h)}$ and $2c = c^{(h)}$). (The dotted line shows the result for $\Delta = 0$ that corresponds to a crack in an infinite homogeneous body; the case $\rho = \rho^{(h)}$ and $c = c^{(h)}$.) This illustrates how, if we fix the material properties of the layer, changes in the half space contribute to the near field. In each case the first reflection, that from the surface $y = 0$ is identical, thereafter if the wavespeed of the half space is slower less energy is reflected towards the crack and the stress intensity factor lies below the dotted (identical materials) line and vice-versa if the half space is faster then it lies above. It is worth noting, that changing the boundary conditions on the crack and on the free surface, may significantly alter the properties of the stress intensity factor.

Finally, in Fig. 5(b), waves are reflected from the surface ($y = 0$) and the interfaces, $y = b_1$, $y = b_2$ at intervals $c_1 t/a = 2$, $c_1 t/a = 2(b_1/a - 1)$, and $c_1 t/a = 2(b_2/a - b_1/a)c_1/c_2 + 2(b_1/a - 1)$, respectively, and combine to generate reflections at all intervals of $c_1 t/a$. In the figure, b_2/a and c_1/c_2 are chosen so that the lower layer first contributes at $c_1 t/a = 5$ and, for ease of presentation, so that the reflections occur at integer values of $c_1 t/a$. ($b_1/a = 5/2$, $b_2/a = 4$, $c_1/c_2 = 2/3$, and $\mu_1 c^{(h)}/\mu^{(h)}c_1 = 1/2$; either $\mu_1 c_2/\mu_2 c_1 = 4$ (—) or

$\mu_1 c_2/\mu_2 c_1 = 1/4$ $(- - -)$ and the $(\cdots)$ shows the result when materials 1 and 2 are identical.) In this figure, we compare the ratios of the moduli in the layers for a fixed ratio of their wavespeeds and demonstrate how similar energy distributions take place.

The semi-infinite result (in an infinite body) is given by the $(\cdot\ -)$ in both panels of Fig. 5.

To explicitly identify the reflections that contribute to the near field expression (3.9) gives

$$\overline{K}(p) = \overline{F}(p)\left(\frac{2c}{p}\right)^{1/2} \sum_{i=0}^{\infty} \frac{(2i)!\Delta^i \mathrm{e}^{-2p(b-a)i/c}}{2^{2i}(i!)^2} \sum_{j=0}^{\infty} \frac{(-1)^{j+1}(2j)!\Delta^j \mathrm{e}^{-2pbj/c}}{(2j-1)2^{2j}(j!)^2} \sum_{k=0}^{\infty} \frac{(-1)^k (2k)! \mathrm{e}^{-2pak/c}}{2^{2k}(k!)^2}, \tag{3.12}$$

which corresponds to the value of K^2 that is deduced from Eq. (2.7). Note that the sign of K cannot be determined without additional information; nonetheless this provides a useful independent check upon one part of the analysis.

We can expand expression (3.12) in orders of the exponential, and this enables us to perform each Laplace inversion term by term to reconstruct the solution in real time explicitly as an infinite series; in particular when $F(t) = H(t)$ and $\Delta = 0$, we obtain

$$K(t) = 2\left(\frac{2c}{\pi}\right)^{1/2} \sum_{k=0}^{\infty} \frac{(-1)^k (2k)!(t-2ka/c)^{1/2} H(t-2ka/c)}{2^{2k}(k!)^2}. \tag{3.13}$$

This is consistent with the solution found numerically. In addition writing the first terms in the series,

$$K(t) = 2\left(\frac{2}{\pi}\right)^{1/2} \left[(ct)^{1/2}H(ct) - \frac{1}{2}(ct-2a)^{1/2}H(ct-2a) + \frac{3}{8}(ct-4a)^{1/2}H(ct-4a) + \cdots\right], \tag{3.14}$$

we can identify these with the coefficients of the singular fields found iteratively in Eqs. (2.18), (2.24), and (2.28) i.e. $K(t) = K^{(0,0)}(t) + K^{(0,1)}(t) + K^{(0,2)}(t) + \cdots$ In Fig. 5(a), the dotted line for $K(t)$ in the interval $0 < ct < 6a$ is given by the first three terms in Eq. (3.14).

4. Weight functions

We have the explicit solution for our model problem of Section 2.1 when the stress loading on the crack is of a simple form; the purpose of this section is to identify the stress intensity factor for any loading using weight functions either for the exact solution, or for the iterative method. Other authors (Thau and Lu, 1971) have utilised iterative methods for related problems; the weight function method carries across to those problems too.

The reciprocal theorem, assuming no body forces are present, is

$$\int_S (\sigma_{ij}^* u_i - \sigma_{ij} u_i^*) n_j \,\mathrm{d}S = 0 \tag{4.1}$$

with n_j the outward pointing normal to the closed surface S. The starred and unstarred fields are independent solutions of the governing equations in the chosen geometry; the starred field is a specially chosen field typically more singular at the crack tip than the physically relevant solution and satisfying zero boundary conditions, that is, it is an eigensolution. Each term in Eq. (4.1) is taken to be in the Laplace transform domain.

For the eigensolution, we consider stresses that are unphysically singular, $\mathrm{O}(r^{-3/2})$, at the crack tip so that in Fourier transform space $\sigma_-^* \sim \mathrm{O}(\xi_-^{1/2})$ as $|\xi| \to \infty$:

$$\sigma_-^* \sim 2^{1/2}\mathrm{i}_-^{-1/2}\xi_-^{1/2}K^*, \qquad U_+^* \sim \frac{2^{3/2}}{\mu}\mathrm{i}_+^{1/2}\xi_+^{-1/2}K^*. \tag{4.2}$$

In our exact formulation of Section 2.1, the functional equation for the eigensolutions is

$$\mu\frac{\gamma_+U_+^*}{\mathscr{Q}_+}=-\frac{\mathscr{Q}_-\sigma_-^*}{\gamma_-}=\mathscr{C}=2\mathrm{i}_+^{1/2}K^*; \tag{4.3}$$

$\mathscr{C}$ is an arbitrary constant which is determined by Liouville's theorem. The value of $\mathscr{C}$ is found by comparison with the known asymptotic form of the near crack tip stresses in Eq. (4.2). Using the reciprocal theorem along a contour applied around the crack tip; the contour then goes along the crack faces and is closed in a large circular arc at infinity,

$$\overline{K}^*(p)\overline{K}(p)=\mu\int_0^\infty\sigma_{zy}(x,a,p)u_z^*(x,a,p)\,\mathrm{d}x. \tag{4.4}$$

As u_z^* emerges from Eq. (4.3), we have a formula for $\overline{K}(p)$:

$$\overline{K}(p)=\frac{1}{2\pi}\mathrm{i}_+^{1/2}\int_0^\infty\sigma_{zy}(x,a,p)\int_{-\infty}^\infty\frac{\mathscr{Q}_+\mathrm{e}^{-\mathrm{i}\xi x}}{\gamma_+}\mathrm{d}\xi\,\mathrm{d}x. \tag{4.5}$$

The application of this formula to the full solution involving product splits of $\mathscr{Q}$ is not a trivial calculation. None the less one can do so and recover the general formula found earlier Eq. (2.9).

We can again proceed in an iterative manner and as a first step this reduces to

$$\frac{\mu}{2^{1/2}}\gamma_+U_+^{*(0,0)}=-2^{1/2}\frac{\sigma_-^{*(0,0)}}{\gamma_-}=\mathscr{C}=2\mathrm{i}_+^{1/2}K^*; \tag{4.6}$$

the formula for the stress intensity factor in this case is given by

$$\overline{K}^{(0,0)}(p)=\frac{1}{2\pi}(2\mathrm{i})_+^{1/2}\int_0^\infty\sigma_{zy}(x,a,p)\int_{-\infty}^\infty\frac{\mathrm{e}^{-\mathrm{i}\xi x}}{\gamma_+}\mathrm{d}\xi\,\mathrm{d}x. \tag{4.7}$$

The particular (Heaviside) loading chosen in the earlier analysis may be recovered using the Fourier transform results given in Appendix A; namely $\overline{K}^{(0,0)}=\overline{F}(p)(2c/p)^{1/2}$. The point of the weight function is that having obtained the solution once for a specific loading, we can utilise the same method to generate eigensolutions; the primary effort in any solution is the factorisation of the 'kernel' function $\mathscr{Q}$. We now choose a loading that is no longer 'uniform' along the crack faces, for instance an exponential loading like $\sigma_{zy}=F(t)\exp(-\lambda x)$, that decays with distance along the crack for positive λ, in which case

$$\overline{K}^{(0,0)}(p)=\overline{F}(p)\left(\frac{2}{p/c+\lambda}\right)^{1/2} \tag{4.8}$$

and when $F(t)=H(t)$ we can find $K^{(0,0)}(t)=(2/\lambda)^{1/2}\mathrm{erf}\sqrt{\lambda ct}$. The uniform loading treated in the previous sections is a special case of this for $\lambda=0$ and we can recover the earlier stress intensity factors.

So far the results have effectively been for a crack in an infinite body; that is the crack is unaware of either the surface or the interface. Next the solutions we have just derived are used to drive the 'reloading' of the unphysically singular crack,

$$\frac{\mu}{2^{1/2}}\gamma_+U_+^{*(0,1)}+2\mathrm{i}_+^{1/2}Q_+^{(0,1)}K^*=-2^{1/2}\frac{\sigma_-^{*(0,1)}}{\gamma_-}-2\mathrm{i}_-^{1/2}Q_-^{(0,1)}K^*=0 \tag{4.9}$$

using $Q_\pm^{(0,1)}\sim\mathrm{O}(1/\xi)\to0$ as $|\xi|\to\infty$. At first sight, it is unclear that the stress or displacement field has the correct *too* singular behaviour. However if, for instance, we consider the stresses, $\sigma^*=\sigma^{*(0,0)}+\sigma^{*(0,1)}+\cdots$, then this expression is still $\mathrm{O}(\xi^{1/2})$ and thus after inversion to the physical domain is still too singular. The stress intensity factor taking into account the first reflection can be found again from applying the reciprocal theorem, and is

$$\overline{K}^{(0,1)}(p) = -\frac{1}{2\pi}(2\mathrm{i})_+^{1/2}\int_0^\infty \sigma_{zy}(x,a,p)\int_{-\infty}^{\infty} Q_+^{(0,1)}\frac{\mathrm{e}^{-\mathrm{i}\xi x}}{\gamma_+}\,\mathrm{d}\xi\,\mathrm{d}x; \tag{4.10}$$

this formula reduces to Eq. (2.24) under a Heaviside loading, making a change of order of integration and then capturing the residue at $\xi = 0$ by closing in the upper half plane.

For further illustration, we again take an exponential loading, $\exp(-\lambda x)$ along the crack faces in which case

$$\overline{K}^{(0,1)}(p) = -\overline{F}(p)\left(\frac{2}{p/c+\lambda}\right)^{1/2}\frac{1}{2}\mathrm{e}^{-2pa/c}, \tag{4.11}$$

and whose inversion for $F(t) = H(t)$ is $K^{(0,1)}(t) = -1/2(2/\lambda)^{1/2}\mathrm{erf}\sqrt{\lambda(ct-2a)}H(ct-2a)$. In Fig. 6 a comparison is made between a uniform and an illustrative non-uniform (exponential) loading for the stress intensity factor. As λ increases the loading decays more rapidly with distance from the crack tip, and the resultant effects on the crack tip stresses are reduced; this is reflected in the reduced stress intensity factor values.

The next solution is given in terms of $Q^{*(0,2)} = Q_+^{(0,1)}Q^{(0,1)} = Q^{(0,2)} - Q_-^{(0,1)}(0)Q^{(0,1)}$, where $Q^{(0,2)}$ is given in Eq. (2.25),

$$\overline{K}^{(0,2)}(p) = -\frac{1}{2\pi}(2\mathrm{i})_+^{1/2}\int_0^\infty \sigma_{zy}(x,a,p)\int_{-\infty}^{\infty} Q_+^{*(0,2)}\frac{\mathrm{e}^{-\mathrm{i}\xi x}}{\gamma_+}\,\mathrm{d}\xi\,\mathrm{d}x; \tag{4.12}$$

for a uniform loading a single residue calculation again recovers our earlier solution. The stress intensity factor for an exponential loading after inversion ($F(t) = H(t)$), shown in Fig. 6, is $K^{(0,2)}(t) = 3/8 \times (2/\lambda)^{1/2}\mathrm{erf}\sqrt{\lambda(ct-4a)}H(ct-4a)$. The combination of formulae $K^{(0,0)}(t) + K^{(0,1)}(t) + K^{(0,2)}(t) + \cdots$ gives a representation for the stress intensity factors which is exact within the time window for which the last

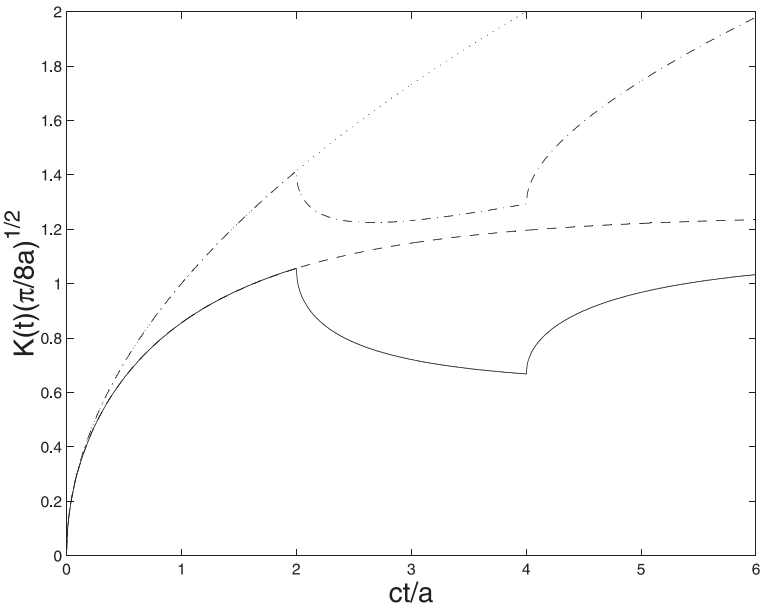

Fig. 6. The stress intensity factors for an exponential loading (—) $\exp(-\lambda x)$ ($\lambda = 0.5/a$) and for a uniform loading (– ·); also shown are the solutions for a crack in an infinite body.

of these is valid. The weight function for waves reflected from the interface between the layer and half space also follows in a similar fashion.

5. In-plane loading

Despite the anti-plane problem of the previous sections being of some independent interest, we are usually more interested in the analogous in-plane problems which we outline in this section. Here there is little success to be had from tackling the problem head-on, unless one wishes to proceed numerically, because of the matrix Wiener–Hopf equation that emerges, however the iterative approach, that we have been advocating so far, is still applicable. There the application of the Cagniard–de Hoop method again avoids any potentially difficult or awkward evaluation of a Fourier and Laplace inverse integral that typically contains a Wiener–Hopf split function. Although the continual reloading of the crack becomes progressively harder to describe.

5.1. Formulation

The problem is already complicated enough without an elastic layer so we only treat a single homogeneous medium with an overlying fluid: In the region $y > 0$ is an isotropic linear elastic material and in $y < 0$ is a compressible fluid. The responses of the two half spaces are coupled together through the continuity boundary conditions along the interface $y = 0$, these are discussed following Eq. (5.2). A Cartesian coordinate system is again adopted with $x_1,\ x_2$ corresponding to $x,\ y$.

The elastic material has (constant) Lamé constants λ, μ, and density ρ. The stresses σ_{ij} in the material are related to the displacements u_i via

$$\sigma_{ij} = \lambda\epsilon_{kk}\delta_{ij} + 2\mu\epsilon_{ij}, \quad \text{where } \epsilon_{ij} = \tfrac{1}{2}(u_{i,j} + u_{j,i}), \tag{5.1}$$

the comma denoting differentiation with respect to x_i. The governing equations are the equilibrium equations $\sigma_{ij,j} = \rho\ddot{u}_i$, where the notation $\ddot{}$ denotes double partial differentiation with respect to time. In this case the analysis is most easily performed by utilising the displacement potentials ϕ and ψ where the displacement $\mathbf{u}$ is $\mathbf{u} = \nabla\phi + \nabla \times \psi\hat{z}$, where $\hat{z}$ is the unit vector in the z direction. The wave speeds c_d, c_s are defined in terms of the material parameters as $c_d^2 = \lambda + 2\mu/\rho$, $c_s^2 = \mu/\rho$. The subscripts d and s denote the variables associated with the dilatational and shear waves respectively.

The compressible fluid in $y < 0$ is effectively an elastic material that supports no shear stresses, thus $\sigma_{ij} = \lambda_f\epsilon_{kk}\delta_{ij}$, where the fluid has density ρ_f and compressional modulus λ_f. The governing equations are $\sigma_{ij,j} = \rho\ddot{u}_i$ again, and we introduce a third displacement potential χ such that the displacement $\mathbf{u}$ is $\mathbf{u} = \nabla\chi$. The compressional wavespeed of the fluid is defined as $c_o^2 = \lambda_f/\rho_f$.

It is useful to define the following γ functions that occur throughout the analysis: $\gamma_q(\xi, p) = (\xi^2 + p^2/c_q^2)^{1/2}$ for $q = d,\ s,\ o,\ r$ where c_r is the Rayleigh wavespeed. A coupling parameter ϵ occurs throughout the analysis and is defined as $\epsilon = \rho_f c_o/\rho c_d$. The assumption that the compressional wavespeed of the fluid is less than the shear wavespeed of the solid is taken so that $c_d > c_s > c_o$.

The following boundary conditions are taken on $y = a$, ahead of, and on, the crack $x > 0$

$$[\![u_x]\!] = [\![u_y]\!] = 0,\ x < 0, \qquad \sigma_{xy} = 0, \qquad \sigma_{yy} = F(t)H(x),\ x > 0, \tag{5.2}$$

and the stresses σ_{xy}, σ_{yy} are continuous across $y = a$: $[\![\sigma_{xy}]\!] = [\![\sigma_{yy}]\!] = 0$. In addition, the continuity boundary conditions

$$[\![\sigma_{yy}]\!] = 0,\ \sigma_{xy} = 0,\ [\![u_y]\!] = 0 \tag{5.3}$$

are taken on the interface $y = 0$, where the braces $[\![\ ]\!]$ denote the jump in a quantity across the interface; both the stresses σ_{yy} and the normal displacement u_y are continuous across $y = 0$. The fluid supports no shear stresses, thus $\sigma_{xy} = 0$ on $y = 0$. For convenience we have, again, taken a spatially uniform loading of the crack faces.

5.2. Transform solution

Once again we apply Fourier and Laplace transforms, this time with the following half-range Fourier transforms: the transform of the unknown stresses, σ_{xy} and σ_{yy}, on $y = a$, $x < 0$,

$$\tau_-(\xi, a, p) = \int_{-\infty}^{0} \overline{\sigma}_{xy}(x, a, p) \mathrm{e}^{\mathrm{i}\xi x}\, \mathrm{d}x, \qquad \sigma_-(\xi, a, p) = \int_{-\infty}^{0} \overline{\sigma}_{yy}(x, a, p) \mathrm{e}^{\mathrm{i}\xi x}\, \mathrm{d}x, \tag{5.4}$$

and the transform of the unknown jump in the displacements, u_x and u_y, across $y = a$, $x > 0$,

$$\begin{aligned} V_+(\xi, a, p) &= \int_0^{\infty} [\overline{u}_x(x, a^+, p) - \overline{u}_x(x, a^-, p)] \mathrm{e}^{\mathrm{i}\xi x}\, \mathrm{d}x, \\ U_+(\xi, a, p) &= \int_0^{\infty} \left[\overline{u}_y(x, a^+, p) - \overline{u}_y(x, a^-, p)\right] \mathrm{e}^{\mathrm{i}\xi x}\, \mathrm{d}x. \end{aligned} \tag{5.5}$$

So far the problems treated have resulted in a single Wiener–Hopf equation like

$$P(\zeta)\Omega_+(\zeta) + Q(\zeta) = \Omega'_-(\zeta), \tag{5.6}$$

and in order to rearrange this equation into the standard Wiener–Hopf form we require only the product factorisation of $P(\zeta) = P_+(\zeta)P_-(\zeta)$. In the present case we obtain a coupled system of two Wiener–Hopf equations and to proceed we need a matrix factorisation. Unfortunately, the components of the matrix do not fall into any of the classes amenable to exact factorisation, and we require some numerical, approximate, or asymptotic method to provide it.

The resulting Wiener–Hopf matrix is

$$\begin{pmatrix} U_+ \\ V_+ \end{pmatrix} = \begin{pmatrix} a_{11} & a_{21} \\ a_{12} & a_{22} \end{pmatrix} \begin{pmatrix} \sigma_- + \Upsilon_+ \\ \tau_- \end{pmatrix}, \quad \text{where } \Upsilon_+ = \frac{\overline{F}(p)}{\mathrm{i}\xi_+}; \tag{5.7}$$

much of the analysis is relegated to the appendices. The expressions for a_{ij} are lengthy and are omitted here; they are written in Appendix C, alternatively we can use the language of generalised ray theory to piece together the matrix. It is our aim to split this equation into a series of elementary Wiener–Hopf equations each of exponential order $\exp[-2m\gamma_d a - 2n\gamma_s a]$. This corresponds to m compressional and n shear reflections against the crack and the fluid-solid interface. The properties of a_{ij} in a Taylor expansion, required to formulate a series of Wiener–Hopf equations are given in Appendix C.

An alternative to approaching the matrix problem head-on is to interpret each reloading separately (Section 2.3). If we do so here, and use displacement potentials, then the potentials that are generated by the first compressional wave that is reflected from the interface are

$$\phi = \left(\mathscr{R}_{pp}\mathrm{e}^{\gamma_d a} + \mathscr{R}_{sp}\mathrm{e}^{\gamma_s a}\right)\mathrm{e}^{-\gamma_d y}, \qquad \psi = \left(\mathscr{R}_{ps}\mathrm{e}^{\gamma_d a} + \mathscr{R}_{ss}\mathrm{e}^{\gamma_s a}\right)\mathrm{e}^{-\gamma_s y}; \tag{5.8}$$

by iteratively constructing those potentials that arise after each reflection one can construct the matrix. In addition if one has, say, a crack obliquely aligned to an interface this method by-passes the necessity of constructing a formal Wiener–Hopf matrix equation. These potentials neatly encapsulate the reflection coefficients ($\mathscr{R}_{pp}$, etc.) that one expects to emerge from a generalised wave expansion and the same functional equations ultimately emerge; this is both algebraically and conceptually easier than dealing with a matrix.

The notation employed in Section 2 is again adopted; the arguments ξ and p are dropped whenever possible. The zero order Wiener–Hopf equation is equivalent to the symmetric problem for a semi-infinite crack in an infinite elastic material, and the corresponding anti-symmetric equation yields $\tau_-^{(0,0)} = 0$:

$$\mu R U_+^{(0,0)} = -2\gamma_d \frac{p^2}{c_s^2}(\sigma_-^{(0,0)} + \Upsilon_+), \qquad \mu R V_+^{(0,0)} = -2\gamma_s \frac{p^2}{c_s^2}\tau_-^{(0,0)}. \tag{5.9}$$

In these formulae R is the standard Rayleigh function, $R(\xi,p) = (\xi^2+\gamma_s^2)^2 - 4\xi^2\gamma_d\gamma_s$. In order to rearrange the symmetric equation into the usual Wiener–Hopf form this function is split into the product of $\pm$ functions. To this end we introduce the function $\mathscr{L}(\xi,p) = \mathscr{L}_+(\xi,p)\mathscr{L}_-(\xi,p)$ defined by Eq. (B.5); the relevant details and expressions are given in Appendix B. Rearranging this functional equation so that the left and right hand sides are analytic in the + and − regions (defined following (2.3)), Eq. (5.9) becomes

$$\begin{aligned} &-\frac{\gamma_{d-}(\xi,p)}{\gamma_{r-}^2(\xi,p)\mathscr{L}_-(\xi,p)}\sigma_-^{(0,0)} - \Upsilon_+\left[\frac{\gamma_{d-}(\xi,p)}{\gamma_{r-}^2(\xi,p)\mathscr{L}_-(\xi,p)} - \frac{\gamma_{d-}(0,p)}{\gamma_{r-}^2(0,p)\mathscr{L}_-(0,p)}\right] \\ &\quad = \mu\left(1-\frac{c_s^2}{c_d^2}\right)\frac{\gamma_{r+}^2(\xi,p)\mathscr{L}_+(\xi,p)}{\gamma_{d+}(\xi,p)}U_+^{(0,0)} + \Upsilon_+\frac{\gamma_{d-}(0,p)}{\gamma_{r-}^2(0,p)\mathscr{L}_-(0,p)} = \Sigma(\xi,p). \end{aligned} \tag{5.10}$$

Analytic continuation may now be invoked to determine that both sides of the functional equation are everywhere equal to the same analytic function, $\Sigma(\xi,p)$. The known edge conditions (i.e. again, the stresses are $O(r^{-1/2})$ there) are now used to determine that this function is in fact zero. This now yields the following expression for the unknown half-range transform, $\sigma_-^{(0,0)}$

$$\sigma_-^{(0,0)} = \Upsilon_+\left[\frac{\gamma_{d-}(0,p)\gamma_{r-}^2(\xi,p)\mathscr{L}_-(\xi,p)}{\gamma_{d-}(\xi,p)\gamma_{r-}^2(0,p)\mathscr{L}_-(0,p)} - 1\right], \tag{5.11}$$

where $\Upsilon_+ = \overline{F}(p)/\mathrm{i}\xi_+$, with a similar result for $U_+^{(0,0)}$.

The behaviour of the stresses near the crack tip may be extracted (using asymptotic results in Appendix B) from Eq. (5.2) as $|\xi| \to \infty$, for $x < 0$:

$$\sigma_{yy}^{(0,0)}(x,a,t) \sim L^{-1}\left[\overline{F}(p)\left(\frac{c_s}{c_d}\right)\left[\frac{2(c_d^2-c_s^2)}{p\pi c_d}\right]^{1/2}(-x)^{-1/2}\right], \qquad \sigma_{xy}^{(0,0)}(x,a,t) \sim 0; \tag{5.12}$$

this result is checked using an invariant integral for the mode I and mode II stress intensity factors K_{I} and K_{II} in Section 5.3.

5.2.1. Reloading by the compressional wave

In this section we consider the reloading of the crack by the compressional wave reflected by the interface. The same procedure may be followed, with some careful attention to the analysis, in extracting the successive Wiener–Hopf equations, to find both the compressional and shear wavefields up to the next arrival. For now we will *only* consider the first reloading of the crack, which for some practical purposes may be thought to be sufficient; further reloadings are briefly examined in Section 5.2.2. An interesting and unexpected result near the crack tip falls out of this analysis and is more rigorously explored in Section 5.3. In order to make use of the Wiener–Hopf equation of exponential order $\exp[-2\gamma_d a]$ we recall that $\tau_-^{(0,0)} = 0$ and therefore from the matrix (5.7), or using the displacement potentials (5.8),

$$\mu R U_+^{(1,0)} = -2\gamma_d \frac{p^2}{c_s^2}\left[\sigma_-^{(1,0)} - \frac{1}{2}\mathscr{R}_{pp}\left(1-\mathscr{R}_{pp}^N\right)\mathrm{e}^{-2\gamma_d a}\left(\sigma_-^{(0,0)} + \Upsilon_+\right)\right]. \tag{5.13}$$

The coefficients $\mathscr{R}$ and $\mathscr{R}^N$ are related to the reflection coefficients for an incident P or S wave on an interface and a surface in the absence of the fluid respectively, and naturally occur in the equations. Their precise form is given in Appendix C.

The corresponding 'anti-symmetric' Wiener–Hopf equation this time yields a non-zero $\tau_-^{(1,0)}$ (that we expect to contribute in the next iteration) from

$$\mu R V_+^{(1,0)} = -2\gamma_s \frac{p^2}{c_s^2}\left[\tau_-^{(1,0)} - \frac{1}{2}\mathscr{R}_{pp}\mathscr{R}_{ps}^N\left(\sigma_-^{(0,0)} + \Upsilon_+\right)\right]. \tag{5.14}$$

Our game plan now requires us to split equation (5.13) into the usual Wiener–Hopf form:

$$-\frac{\gamma_{d-}(\xi,p)}{\gamma_{r-}^2(\xi,p)\mathscr{L}_-(\xi,p)}\sigma_-^{(1,0)} - \Upsilon_+\Theta(\xi,p)\frac{\gamma_{d-}(0,p)}{\gamma_{r-}^2(0,p)\mathscr{L}_-(0,p)} = \mu\left(1-\frac{c_s^2}{c_d^2}\right)\frac{\gamma_{r+}^2(\xi,p)\mathscr{L}_+(\xi,p)}{\gamma_{d+}(\xi,p)}U_+^{(1,0)}. \tag{5.15}$$

We have taken in hand the sum split of $\Theta(\xi,p)$ into a + function and a − function:

$$\Theta(\xi,p) = -\tfrac{1}{2}\mathscr{R}_{pp}(1-\mathscr{R}_{pp}^N)\mathrm{e}^{-2\gamma_d(\xi,p)a} = \Theta_+(\xi,p) + \Theta_-(\xi,p); \tag{5.16}$$

some consideration of the function reveals that $\Theta_+(\xi,p) = \Theta_-(-\xi,p)$ and therefore $2\Theta_\pm(0,p) = \Theta(0,p) = [(1-\epsilon)/(1+\epsilon)]\mathrm{e}^{-2pa/c_d}$, which will be seen to be useful later. The resulting functional equation yields the unknown stress transform:

$$\sigma_-^{(1,0)} = -\Upsilon_+\frac{\gamma_{d-}(0,p)\gamma_{r-}^2(\xi,p)\mathscr{L}_-(\xi,p)}{\gamma_{d-}(\xi,p)\gamma_{r-}^2(0,p)\mathscr{L}_-(0,p)}[\Theta_-(\xi,p) - \Theta_-(0,p)], \tag{5.17}$$

and we extract the stress intensity factor by employing asymptotic result $\Theta_-(\xi,p) \to \mathrm{O}(1/\xi)$ as $\xi \to \infty$, i.e.

$$\sigma_{yy}^{(1,0)}(x,a,t) \sim L^{-1}\left[\overline{F}(p)\left(\frac{c_s}{c_d}\right)\left[\frac{2\left(c_d^2-c_s^2\right)}{p\pi c_d}\right]^{1/2}\Theta_-(0,p)(-x)^{-1/2}\right];$$

$$\Theta_-(0,p) = \frac{1}{2}\frac{(1-\epsilon)}{(1+\epsilon)}\mathrm{e}^{-2pa/c_d}. \tag{5.18}$$

We may now use this result to find the mode I stress intensity factor, $\overline{K}_\mathrm{I}(p)$. In addition, the mode II stress intensity factor may be found, in a similar manner, by first setting

$$\Phi(\xi,p) = -\frac{\gamma_{s-}}{2\gamma_{d-}}\mathscr{R}_{pp}\mathscr{R}_{ps}^N\mathrm{e}^{-2\gamma_d(\xi,p)a} = \Phi_+(\xi,p) + \Phi_-(\xi,p). \tag{5.19}$$

The functional equation then yields

$$\tau_-^{(1,0)} = -\Upsilon_+\frac{\gamma_{d-}(0,p)\gamma_{r-}^2(\xi,p)L_-(\xi,p)}{\gamma_{s-}(\xi,p)\gamma_{r-}^2(0,p)L_-(0,p)}[\Phi_-(\xi,p) - \Phi_-(0,p)], \tag{5.20}$$

and we may extract the stress intensity factor utilising $\Phi_-(\xi,p) \sim \mathrm{O}(1/\xi)$ as

$$\sigma_{xy}^{(1,0)}(x,a,t) \sim L^{-1}\left[\overline{F}(p)\left(\frac{c_s}{c_d}\right)\left[\frac{2\left(c_d^2-c_s^2\right)}{p\pi c_d}\right]^{1/2}\Phi_-(0,p)(-x)^{-1/2}\right]; \qquad \Phi_-(0,p) \equiv 0, \tag{5.21}$$

as $\Phi(0,p) = \Phi_\pm(0,p) = 0$. As a consequence of this result the mode II stress intensity factor is zero, at least until the next wave reloads the crack; without the fluid loading and for a stationary crack a similar result is found by Tsai and Ma (1997). This is consistent with the invariant integral that we use in Section 5.3; there we conclude that the zero mode II intensity factor is a result of the specific stress loading we have taken on the crack faces.

We may pursue a modified Cagniard method again to explicitly determine the stress fields anywhere in the fluid or solid, using these results for unknown transforms and closely following the analysis in Section 2.2. Alternatively, as it is this the case here, we may further investigate the stress intensity factors. We have seen, when treating the anti-plane example, that this is often best achieved using an invariant integral. First,

we briefly examine the effect near the crack tip, of some other waves reloading the crack using our iterative approach.

5.2.2. Reloadings by other waves

The crack is also reloaded by mode-converted and shear waves reflected by the interface whose contributions to the stress field may be found from the following functional equations:

- *SP wave*

$$\begin{aligned}\mu R U_+^{(1,1)a} &= -2\gamma_d \frac{p^2}{c_s^2}\left[\sigma_-^{(1,1)a} - \frac{1}{2}\mathscr{R}_{ps}\mathscr{R}_{sp}^N \mathrm{e}^{-\gamma_d a-\gamma_s a}\left(\sigma_-^{(0,0)}+\Upsilon_+\right)\right],\\ \mu R V_+^{(1,1)a} &= -2\gamma_s \frac{p^2}{c_s^2}\left[\tau_-^{(1,1)a} + \frac{1}{2}\mathscr{R}_{ps}\left(1+\mathscr{R}_{ss}^N\right)\mathrm{e}^{-\gamma_d a-\gamma_s a}\left(\sigma_-^{(0,0)}+\Upsilon_+\right)\right];\end{aligned} \tag{5.22}$$

- *PS wave*

$$\begin{aligned}\mu R U_+^{(1,1)b} &= -2\gamma_d \frac{p^2}{c_s^2}\left[\sigma_-^{(1,1)b} - \frac{1}{2}\mathscr{R}_{sp}\mathscr{R}_{ps}^N \mathrm{e}^{-\gamma_d a-\gamma_s a}\left(\sigma_-^{(0,0)}+\Upsilon_+\right)\right],\\ \mu R V_+^{(1,1)b} &= -2\gamma_s \frac{p^2}{c_s^2}\left[\tau_-^{(1,1)b} - \frac{1}{2}\mathscr{R}_{ps}\left(1-\mathscr{R}_{ss}^N\right)\mathrm{e}^{-\gamma_d a-\gamma_s a}\left(\sigma_-^{(0,0)}+\Upsilon_+\right)\right];\end{aligned} \tag{5.23}$$

- *SS wave*

$$\begin{aligned}\mu R U_+^{(0,1)} &= -2\gamma_d \frac{p^2}{c_s^2}\left[\sigma_-^{(0,1)} + \frac{1}{2}\mathscr{R}_{ss}\left(1+\mathscr{R}_{ss}^N\right)\mathrm{e}^{-2\gamma_s a}\left(\sigma_-^{(0,0)}+\Upsilon_+\right)\right],\\ \mu R V_+^{(0,1)} &= -2\gamma_s \frac{p^2}{c_s^2}\left[\tau_-^{(0,1)} - \frac{1}{2}\mathscr{R}_{ss}\mathscr{R}_{ps}^N \mathrm{e}^{-2\gamma_s a}\left(\sigma_-^{(0,0)}+\Upsilon_+\right)\right].\end{aligned} \tag{5.24}$$

There are two mode-converted waves (*SP* and *PS*) that reload the crack and some physical considerations are required to extract these equations separately from the matrix expansion (C.9)–(C.11) in Appendix C. In each of these Eqs. (5.22)–(5.24), the function to be split in order to make the correct combination of + and − functions is somewhat akin to Φ defined in Eq. (5.19) in that it is zero at the pole situated at $\xi_+ = 0_+$. Then, as in that case, some consideration of the ± functions implies that they too are zero. Ultimately, this means that both the mode I and mode II stress intensity factors are zero for each of these successive reloadings.

A more complete picture for the stress intensity factors is given in Section 5.3. That section suggests that we *only* expect to find a non-zero contribution near the crack tip from purely compressional reloadings on the crack. This multiply reflected wave becomes increasingly difficult to describe in our iterative language. However, there are simplifications that occur in the limit as $\xi \to \infty$ that we can take advantage of to find $\overline{K_{\mathrm{I}}}(p)$ directly. The functional equation in this case is

$$\begin{aligned}\mu R U_+^{(2,0)} = -2\gamma_d \frac{p^2}{c_s^2}\Bigg[&\sigma_-^{(2,0)} - \frac{1}{2}\mathscr{R}_{pp}\left(1-\mathscr{R}_{pp}^N\right)\mathrm{e}^{-2\gamma_d a}\sigma_-^{(1,0)} - \frac{1}{2}\mathscr{R}_{pp}\mathscr{R}_{sp}^N \mathrm{e}^{-2\gamma_s a}\tau_-^{(1,0)}\\ &- \frac{1}{2}\mathscr{R}_{pp}\mathscr{R}_{pp}^N\mathscr{R}_{pp}\left(1-\mathscr{R}_{pp}^N\right)\mathrm{e}^{-4\gamma_d a}\left(\sigma_-^{(0,0)}+\Upsilon_+\right)\Bigg].\end{aligned} \tag{5.25}$$

so that the equality of a + and − function is ultimately given in terms of the sum split of Ψ:

$$\Psi = \frac{1}{2}\mathscr{R}_{pp}\left(1-\mathscr{R}^N_{pp}\right)\mathrm{e}^{-2\gamma_d a}[\Theta_-(\xi,p)-\Theta_-(0,p)] + \frac{\gamma_{d-}}{2\gamma_{s-}}\mathscr{R}_{pp}\mathscr{R}^N_{sp}\mathrm{e}^{-2\gamma_s a}[\Phi_-(\xi,p)-\Phi_-(0,p)]$$
$$-\frac{1}{2}\mathscr{R}_{pp}\mathscr{R}^N_{pp}\mathscr{R}_{pp}\left(1-\mathscr{R}^N_{pp}\right)\mathrm{e}^{-4\gamma_d a}$$
$$= \Psi_+(\xi,p)+\Psi_-(\xi,p); \tag{5.26}$$

the stress intensity factor is found by evaluating $\Psi_-(0,p) = I_\Psi + [\Theta_-(0,p)]^2$, the other pieces of Ψ do not contribute. The integral I_Ψ is found to be

$$I_\Psi = \frac{1}{2\pi\mathrm{i}}\int_{-\infty+\mathrm{i}d}^{\infty+\mathrm{i}d}\Theta(\eta,p)\Theta_-(\eta,p)\frac{\mathrm{d}\eta}{\eta} = \frac{1}{8}\left(\frac{1-\epsilon}{1+\epsilon}\right)^2\mathrm{e}^{-4pa/c_d}, \tag{5.27}$$

and this result gives the value of K_I, also found in the following section.

5.3. Invariant integral

In the previous section, we observed that the mode II intensity factor for this specific loading is zero to $\mathrm{O}(\mathrm{e}^{-2\gamma_d a})$. This is perhaps unexpected and is verified in this section using an invariant integral, together with some extensions to non-homogeneous media. More general loadings, using a weight function, are not considered here but could be treated as in Section 4.

Following the approach used in Section 3 a Lagrangian is, this time, deduced in each half space (fluid and solid) such that the Euler–Lagrange relations recover the governing equations. In the elastic material, the Lagrangian L is defined as

$$L = -\tfrac{1}{2}\left(\overline{\sigma}_{ij}\overline{u}_{i,j} + \rho p^2\overline{u}_i\overline{u}_i\right), \tag{5.28}$$

and in the fluid half space $L^{(f)}$ is the same expression with superscripts (f) used to denote displacements and stresses in the fluid and ρ replaced by ρ_f. The pseudo energy momentum tensor P_{lj} is formed in the usual manner, i.e.

$$P_{lj} = \frac{\partial L}{\partial\overline{u}_{i,j}}\overline{u}_{i,l} - L\delta_{lj}. \tag{5.29}$$

This pseudo energy momentum tensor has $P_{lj,j} = 0$ so that the integrals defined by F_l are invariant. We should note, see Atkinson and Craster (1995a), that closing a contour around a crack tip gives a term involving $\overline{K}^2_\mathrm{I}(p) + \overline{K}^2_\mathrm{II}(p)$ and the physical significance of this result is not clear. Nevertheless, this is a valuable check on our, or further, numerical work. The designation I or II indicates the independent contribution due to crack extension in mode I or mode II.

The integrals defined as

$$F_\mathrm{I} = \int_S P_{1j}n_j\,\mathrm{d}S = \int_S\left[-\overline{\sigma}_{ij}n_j\overline{u}_{i,1} + \frac{1}{2}\left(\overline{\sigma}_{ij}\overline{u}_{i,j} + \rho p^2\overline{u}_i\overline{u}_i\right)n_1\right]\mathrm{d}S \tag{5.30}$$

are zero provided the path S (Fig. 7) does not enclose any singularities and the path remains in the material for which P_{1j} is defined. In this formula n_j is the unit vector normal to S. The integral $F_\mathrm{I} = F_\mathrm{I} + F_\mathrm{I}^{(f)}$ is considered around the contour shown in Fig. 7; the paths in the fluid and the solid have the interface in common. Near edge fields are used to evaluate the integral around GH in Fig. 7. The only other integrals that contribute to the invariant are along EF, AB, and $F'E'$ (in the fluid), and the points at F and A along the crack faces. The stresses at a crack tip are singular, i.e. $\sigma \sim KG(\theta)r^{-1/2}$, where r and θ are polar coordinates based at the crack tip; see Atkinson and Craster (1995b) among others.

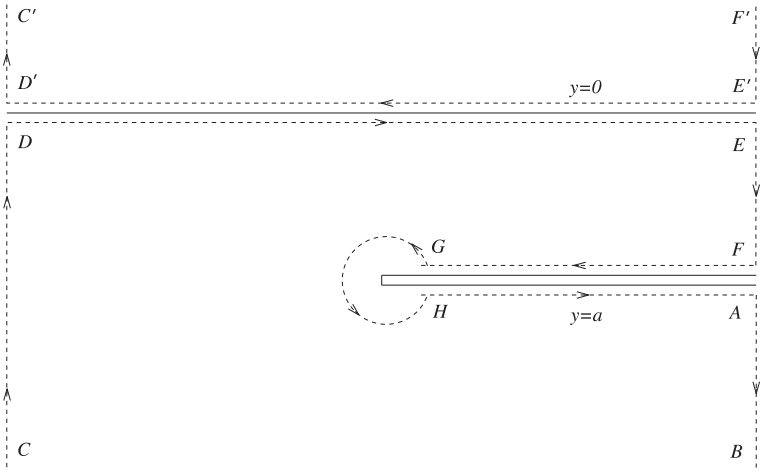

Fig. 7. The path, S, required for the application of the invariant integral in Section 5.

Performing integrals gives

$$\frac{(1-\nu^2)}{E}(\overline{K}_{\mathrm{I}}^2+\overline{K}_{\mathrm{II}}^2)(p)=\frac{\overline{F}^2(p)}{p}\,\frac{1}{2\rho c_d}(\epsilon+1)\,\frac{\left(\cosh\frac{pa}{c_d}+\sinh\frac{pa}{c_d}\right)}{\left(\epsilon\cosh\frac{pa}{c_d}+\sinh\frac{pa}{c_d}\right)}, \tag{5.31}$$

where E is Young's modulus and ν is the Poisson's ratio; E and ν are related to the shear modulus μ and the wavespeeds c_d, c_s by $(1-\nu^2)/E=c_d^2/4\mu(c_d^2-c_s^2)$. The stress intensity factor in $0<c_dt/a<2$ is the first term in the expansion,

$$\overline{K}_{\mathrm{I}}(p)=2\overline{F}(p)\left(\frac{c_s}{c_d}\right)\left(\frac{c_d^2-c_s^2}{pc_d}\right)^{1/2}\left[1+\frac{1}{2}\left(\frac{1-\epsilon}{1+\epsilon}\right)\mathrm{e}^{-2pa/c_d}+\frac{3}{8}\left(\frac{1-\epsilon}{1+\epsilon}\right)^2\mathrm{e}^{-4pa/c_d}+\cdots\right]. \tag{5.32}$$

This result corresponds to the value of $\overline{K}_{\mathrm{I}}$ that is deduced from Eq. (5.12). The second term is also consistent with Eq. (5.18). This provides a useful independent check upon one part of our analysis. It is noteworthy that these results are the same as those we would obtain if we had 'pre-fractured' the plane $y=a$, and therefore $\sigma_{xy}=0$ for all x along $y=a$. In that case, one only extracts a mode I stress intensity factor $\overline{K}_{\mathrm{I}}$ using the invariant rather than the sum of the squares of both intensity factors. Apart from a term which comes from the time dependence of the crack loading, the result in Eq. (5.31) only includes the compressional wavespeed suggesting that no shear waves reload the crack in such a way as to induce singular shear stresses at the crack tip. Hence, we conjecture that for the specific 'opening' loading on the crack then, in fact, K_{II} is zero for all time. Further inspection of the iterative scheme confirms this.

Similarly for a 'shearing' loading on the crack, like $\sigma_{yy}=0$, $\sigma_{xy}=F(t)$ on $y=a$, $x>0$, then we find the combination of stress intensity factors to be

$$\frac{(1-\nu^2)}{E}(\overline{K}_{\mathrm{I}}^2+\overline{K}_{\mathrm{II}}^2)(p)=\frac{\overline{F}^2(p)}{p}\,\frac{1}{2\rho c_s}\,\frac{\left(\cosh\frac{pa}{c_s}+\sinh\frac{pa}{c_s}\right)}{\sinh\frac{pa}{c_s}}, \tag{5.33}$$

and this time K_{I} is zero.

The stress intensity factor $(c_s/c_d)(1-c_s^2/c_d^2)^{1/2}K^R(t)=[K_{\mathrm{I}}^2(t)+K_{\mathrm{II}}^2(t)]^{1/2}(\pi/16a)^{1/2}$ versus non-dimensional time c_dt/a is shown in Fig. 8. In panel (a) of this figure, we compare the stress intensity factors under

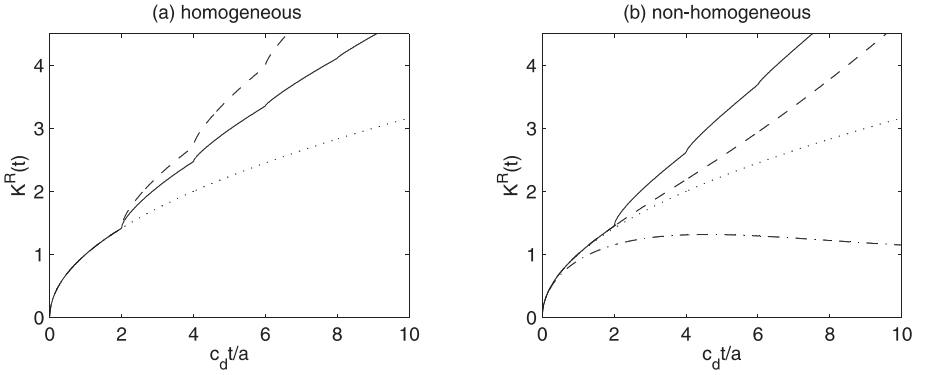

Fig. 8. Rescaled stress intensity factors for homogeneous and non-homogeneous materials; see text for details.

moderate, $\epsilon = 0.2$ (—), and zero, $\epsilon = 0$ (– – –), fluid loading, and we can see that the effect of the fluid is to draw energy away leading to less reflected back towards the crack. In contrast to the anti-plane results in Figs. 4 and 5 which were for a crack beneath a rigid surface, the stress continuity conditions on the interface have reloaded the crack in such a way as to increase the stress intensity factor with each successive re-loading. The result for a crack in an infinite elastic material is shown by the dotted line (· · ·).

The organisation of this section has primarily been to investigate the stress intensity factors of the previous section, and hence, a homogeneous cracked elastic half-space coupled to an overlying fluid. But there is nothing to stop us, bar some unpleasant algebra, from looking at non-homogeneous materials; for simple analytical results the moduli variations in the y direction are best given specific forms. For example, if we choose $\lambda(y) = \lambda_0 e^{2\beta y}$, $\mu(y) = \mu_0 e^{2\beta y}$, and $\lambda_f(y) = \lambda_{f0} e^{2\beta_f y}$ to vary in such a way that c_d, c_s, and c_o are all constant, then the square of the stress intensity factors is

$$\frac{(1-\nu^2)}{E}\left(\overline{K}_{\mathrm{I}}^2(p) + \overline{K}_{\mathrm{II}}^2(p)\right) = \frac{\overline{F}^2(p)}{2(\lambda+2\mu)(a)}\left[\frac{1}{(\Gamma_d+\beta)} - \left(\frac{(\beta+\mathscr{E}\Gamma_d)\sinh\Gamma_d a + \Gamma_d\cosh\Gamma_d a}{(\beta^2+\mathscr{E}\beta\Gamma_d-\Gamma_d^2)\sinh\Gamma_d a - \mathscr{E}\Gamma_d^2\cosh\Gamma_d a}\right)\right], \tag{5.34}$$

where

$$\mathscr{E} = \frac{\lambda_{f0}(\Gamma_0-\beta_f)}{(\lambda_0+2\mu_0)\Gamma_d} \qquad (= \epsilon \text{ when } \beta=\beta_f=0), \tag{5.35}$$

and we have defined $\Gamma_d = (p^2/c_d^2+\beta^2)$ and $\Gamma_0 = (p^2/c_o^2+\beta_f^2)$. As in Section 3, if we now choose $\lambda(y) = \lambda_0 e^{2\beta|y-a|}$ and $\mu(y) = \mu_0 e^{2\beta|y-a|}$ in an infinite elastic body then we find for such a symmetric variation

$$\overline{K}_{\mathrm{I}}(p) = 2\overline{F}(p)\left(\frac{c_s}{c_d}\right)\left[\frac{c_d^2-c_s^2}{(\Gamma_d+\beta)c_d^2}\right]^{1/2}. \tag{5.36}$$

The stress intensity factor in Eq. (5.34) when $\beta = 0.3/a$, $\beta_0 = 0.1c_d/c_o a$, and $\epsilon = \lambda_{f0}c_d/(\lambda_0+2\mu_0)c_o = 0.2$ is shown in panel (b) of Fig. 8. The results in an infinite body are also compared for this inhomogeneity (– – –) and replacing the y dependence of each parameter by $|y-a|$ to make it symmetric about the crack (– ·); the dotted line is when the material is homogeneous as in panel (a). This result (Fig. 8(b)) again demonstrates how the effect of inhomogeneity can be to increase or decrease the stress intensity factors. In the latter case, when the material variation is such that the crack, in effect, appears to be within a strip bounded by rigid walls. It is worth noting that the special situation of a crack centred in a strip (Atkinson and Craster, 1992b)

with either symmetric, or anti-symmetric, loadings applied to the strip walls is a special case, here the invariant extracts the stress intensity factor (and there is now only one factor due to the complete symmetry or anti-symmetry of the problem) in a particularly neat and concise manner.

6. Conclusion

An efficient method based on both physical considerations and an iterative approach to the underlying Wiener–Hopf equation(s) for scattering by a crack is demonstrated in this study. In essence, the equation is broken into smaller pieces, using generalised ray theory, that capture the wavefield within a finite time window. Of course it is necessary to pose and solve a series of Wiener–Hopf equations, and this procedure can become progressively more involved.

To illustrate the scope of the method, we have applied it to both anti-plane and in-plane loadings of a crack, and extracted the stress fields and the stress intensity factors. It is noted that for a specific class of in-plane loadings on the crack, namely a spatially constant pure 'opening' or 'shearing', there is no complementary shearing or opening piece of the stress intensity factors.

A second route taken in this paper is to use an invariant integral to extract the stress intensity factors directly. This is, in part, an independent check on the results. It also permits some extensions to non-homogeneous media, where our other approach is less feasible. Some illustrative results are given and it is anticipated that the general methodology will carry over to problems of a harder nature. The effect of the inhomogeneity is, of course, dependent on the precise nature of the variation as one moves away from the crack, and we demonstrate some contrasting behaviour in the stress intensity factors dependent upon whether the modulus decreases or increases with distance away from the fracture plane.

Specifically, for either stress free or rigid boundary conditions the reloading on the crack faces reinforces the initial opening stress or it stifles the opening. The non-homogeneous moduli do this in a 'continuous' way rather than via the discrete reflections of a layered material.

Acknowledgements

The authors would like to thank the EPSRC for providing funding via an Advanced Fellowship (R.V.C) and a Research Studentship (D.P.W). The authors are also grateful to the referees for their helpful and useful comments.

Appendix A. Fourier transform results

If F denotes the Fourier transform operator, then

$$F^{-1}\left(\frac{1}{\xi_+^{n+1/2}}\right)=\frac{(x)^{n-1/2}H(x)}{\mathrm{i}_+^{n+1/2}\Gamma(n+1/2)}, \tag{A.1}$$

where n is an integer, and $\Gamma(z)$ is the Gamma function defined to be $\Gamma(n+1)=\int_0^\infty t^n\mathrm{e}^{-t}\,\mathrm{d}t$.

Appendix B. Product splits

In Section 2.1, we have taken in hand the product split of $\mathscr{Q}(\xi,p)$ (see Eq. (2.5)). This function is split into $+$ and $-$ functions that are analytic and non-zero in the upper and lower complex ξ planes: $\mathscr{Q}(\xi,p)=\mathscr{Q}_+(\xi,p)\mathscr{Q}_-(\xi,p)$,

$$\log \mathscr{Q}_-(\xi,p) = -\frac{1}{2\pi \mathrm{i}} \int_{-\infty+\mathrm{i}d}^{\infty+\mathrm{i}d} \frac{\log \mathscr{Q}(\eta,p)}{\eta-\xi}\mathrm{d}\eta \qquad \log \mathscr{Q}_+(\xi,p) = \frac{1}{2\pi \mathrm{i}} \int_{-\infty-\mathrm{i}d}^{\infty-\mathrm{i}d} \frac{\log \mathscr{Q}(\eta,p)}{\eta-\xi}\mathrm{d}\eta \tag{B.1}$$

for $-d < \mathrm{Im}(\xi) < d$, where d is some small, positive, real number. It is adequate, in most cases, to compute this product split numerically, and this is most easily performed using quadratures.

There is a useful limit as $b \to \infty$ that permits some explicit formulae to be derived. In this case, the function to be split into a product of $\pm$ functions is $\mathscr{Q}^*(\xi,p) = \mathrm{e}^{\gamma(\xi,p)a}/\cosh(\gamma(\xi,p)a)$, and these be constructed analytically. The factorisation can be achieved by considering separately the factorisations of $\mathrm{e}^{-\gamma a}$ and $\cosh \gamma a$, and has the familiar form (Noble, 1958),

$$\frac{1}{\mathscr{Q}^*_+}(\xi,p) = \mathrm{e}^{-\chi(\xi,p)-\psi_+(\xi,p)} \prod_{n=0}^{\infty} \left[(1+p^2a_{n-1/2}^2c^{-2})^{1/2} - \mathrm{i}\xi a_{n-1/2}\right] \mathrm{e}^{\mathrm{i}\xi a_{n-1/2}}, \tag{B.2}$$

where $a_{n-1/2} = a/(n-(1/2))\pi$, $\mathscr{Q}^*_-(\xi,p) = \mathscr{Q}^*_+(-\xi,p)$ and

$$\psi_+(\xi,p) = \frac{a}{\pi}\left(\xi^2 + \frac{p^2}{c^2}\right)^{1/2} \cos^{-1}\left(-\mathrm{i}\frac{\xi c}{p}\right), \qquad \psi_-(\xi,p) = \psi_+(-\xi,p). \tag{B.3}$$

In Eq. (B.2) $\chi(\xi,p)$ is an arbitrary function chosen so that $\mathscr{Q}^*_+$ and $\mathscr{Q}^*_-$ have polynomial behaviour at infinity. Thus, using well known properties of the gamma function, we choose

$$\chi(\xi,p) = -\mathrm{i}\frac{\xi a}{\pi}\left[1-\gamma+\log\left(-\mathrm{i}\frac{\pi c}{2ap}\right)\right] + \frac{\xi a}{2}, \tag{B.4}$$

where in Eq. (B.4) γ is Euler's constant. In practice, we can avoid these splits by using the modified Cagniard method.

The Wiener–Hopf method in Section 5 requires the product split of the Rayleigh function, $R(\zeta)$, suitably rescaled. To split this Rayleigh function first consider a new function $\mathscr{L}(\zeta)$ (that appears in Section 5),

$$\mathscr{L}(\zeta) = \frac{(2\zeta^2+k^2)^2 - 4\zeta^2(\zeta^2+1)^{1/2}(\zeta^2+k^2)^{1/2}}{2(k^2-1)(\zeta^2+k_r^2)}; \tag{B.5}$$

the product splits for $R(\zeta)$ follow directly from those of $\mathscr{L}(\zeta)$: $\mathscr{L}(\zeta) = \mathscr{L}_+(\zeta)\mathscr{L}_-(\zeta)$. By introducing the branch cuts $\mathrm{Re}(\zeta) = 0$, $1 < |\mathrm{Im}(\zeta)| < k$, $\mathscr{L}(\zeta)$ is made analytic everywhere in this cut ζ plane. The following asymptotic property is useful: in the limit as $|\zeta| \to \infty$, $\mathscr{L}(\zeta) \to 1 + \mathrm{O}(\zeta^{-2})$. These properties of $\mathscr{L}(\zeta)$ make the logarithmic function $\log \mathscr{L}(\zeta)$ analytic everywhere in the same cut ζ plane as $\mathscr{L}(\zeta)$ and ensures that the Cauchy integrals converge. Using Cauchy's theorem $\mathscr{L}_-(\zeta)$ is determined explicitly as

$$\log \mathscr{L}_-(\zeta) = -\frac{1}{\pi}\int_1^k \tan^{-1}\left[\frac{4\tau^2(\tau^2-1)^{1/2}(k^2-\tau^2)^{1/2}}{(k^2-2\tau^2)^2}\right]\frac{\mathrm{d}\tau}{\tau+\mathrm{i}\zeta}, \tag{B.6}$$

where $\mathscr{L}_+(\zeta) = \mathscr{L}_-(-\zeta)$ and the branch of the inverse tangent is chosen so that $0 \leqslant \tan^{-1}\phi \leqslant \pi/2$. Some further asymptotic properties of $\mathscr{L}_+(\zeta)$ are useful when we come to consider the stress intensity factors: as $|\zeta| \to \infty$ then $\mathscr{L}_+(\zeta) \to 1$, and $\mathscr{L}_+(0) = k^2/[2^{1/2}(k^2-1)^{1/2}k_r]$. Then we have

$$R_-(\zeta) = 2^{1/2}(k^2-1)^{1/2}\gamma_{r-}^2(\xi,p)\mathscr{L}_-(\xi,p); \tag{B.7}$$

a rescaling by $\xi = p\zeta/c$ and $k = c_d/c_s$ is required in the main text.

In more general diffraction problems the kernel function is split similar to the above fundamental procedure, although often explicit formulae are not forthcoming.

Appendix C. Reflection coefficients and Wiener–Hopf notation

In the first part to this appendix, the coefficients $\mathscr{R}$ and $\mathscr{R}^N$ are related to the reflection coefficients for an incident P or S wave on an interface and a surface in the absence of the fluid, respectively (the superscript N denotes no fluid). The subscripts on $\mathscr{R}$ and $\mathscr{R}^N$ follow the convention that the first denotes the type of incident wave and the second denotes the type of reflected wave.

There are related transmission coefficients, and coefficients given by incident waves from the fluid, but these are not required in the application considered in the text.

In the following, the usual notation is used for the Rayleigh, $R(\xi)$, and Schölte, $S(\xi)$, functions and also their complements $r(\xi)$ and $s(\xi)$:

$$\begin{aligned} R(\xi) &= \left[\xi^2+\gamma_s^2(\xi)\right]^2 - 4\xi^2\gamma_d(\xi)\gamma_s(\xi), \qquad S(\xi) = R(\xi) + \epsilon\gamma_d(\xi)/\gamma_o(\xi), \\ r(\xi) &= \left[\xi^2+\gamma_s^2(\xi)\right]^2 + 4\xi^2\gamma_d(\xi)\gamma_s(\xi), \qquad s(\xi) = r(\xi) - \epsilon\gamma_d(\xi)/\gamma_o(\xi). \end{aligned} \tag{C.1}$$

The Laplace transform parameter, p, dependence has been omitted for ease of presentation.

- *Incident P wave:*

$$\begin{aligned} &\mathscr{R}_{pp} = -\frac{s(\xi)}{S(\xi)}, \qquad \mathscr{R}_{ps} = \frac{4\mathrm{i}\xi\gamma_d(\xi)[\xi^2+\gamma_s^2(\xi)]}{S(\xi)}, \qquad \mathscr{R}^N_{pp} = -\frac{r(\xi)}{R(\xi)}, \\ &\mathscr{R}^N_{ps} = \frac{4\mathrm{i}\xi\gamma_d(\xi)[\xi^2+\gamma_s^2(\xi)]}{R(\xi)}. \end{aligned} \tag{C.2}$$

- *Incident S wave:*

$$\begin{aligned} &\mathscr{R}_{sp} = -\frac{4\mathrm{i}\xi\gamma_s(\xi)[\xi^2+\gamma_s^2(\xi)]}{S(\xi)}, \qquad \mathscr{R}_{ss} = -\frac{S(\xi)+8\xi^2\gamma_s(\xi)\gamma_d(\xi)}{S(\xi)}, \\ &\mathscr{R}^N_{sp} = -\frac{4\mathrm{i}\xi\gamma_s(\xi)[\xi^2+\gamma_s^2(\xi)]}{R(\xi)}, \qquad \mathscr{R}^N_{ss} = -\frac{r(\xi)}{R(\xi)}. \end{aligned} \tag{C.3}$$

In Section 5, the problem reduces to the solution of a Wiener–Hopf matrix (5.7):

$$\begin{pmatrix} U_+ \\ V_+ \end{pmatrix} = \begin{pmatrix} a_{11} & a_{12} \\ a_{21} & a_{22} \end{pmatrix} \begin{pmatrix} \sigma_- + \Upsilon_+ \\ \tau_- \end{pmatrix}. \tag{C.4}$$

It is unfortunately the case that the matrix terms a_{ij} become rather ugly, and as noted in the text we can piece together the matrix in orders of the exponential using generalised ray theory. Alternatively, we can deal with the matrix and perform a series of expansions. The latter route is taken here:

$$\mu a_{11} = -\gamma_d \frac{p^2}{c_s^2}\left[\frac{1}{R} + \frac{1}{\mathscr{K}}\left(S + s\mathrm{e}^{-2\gamma_d a} - (S+8\xi^2\gamma_s^2\gamma_d^2)\mathrm{e}^{-2\gamma_s a} - (s-8\xi^2\gamma_s\gamma_d)\mathrm{e}^{-2(\gamma_d+\gamma_s)a}\right)\right], \tag{C.5}$$

where

$$\mathscr{K} = SR - sr\mathrm{e}^{-2\gamma_d a} - (S+8\xi^2\gamma_s^2\gamma_d^2)r\mathrm{e}^{-2\gamma_s a} + (s-8\xi^2\gamma_s\gamma_d)R\mathrm{e}^{-2(\gamma_d+\gamma_s)a} + 32\xi^2\gamma_s\gamma_d(\xi^2+\gamma_s^2)^2\mathrm{e}^{-(\gamma_d+\gamma_s)a}. \tag{C.6}$$

Note that in the case of a pre-fractured crack where the boundary condition ahead of the crack is $\sigma_{xy} = 0$ so that the shear stresses are zero all along $y = a$, then the Wiener–Hopf equation (5.7) reduces to $U_+ = a_{11}(\sigma_- + \Upsilon_+)$. The remaining components are as follows:

$$\mu a_{12} = -\mu a_{21}$$
$$= \mathrm{i}\xi\left[\frac{q_2}{R} - \frac{1}{\mathscr{K}}\left(q_2 S - s q_1 \mathrm{e}^{-2\gamma_d a} - (S + 8\xi^2\gamma_s\gamma_d) q_1 \mathrm{e}^{-2\gamma_s a} + (s - 8\xi^2\gamma_s\gamma_d) q_2 \mathrm{e}^{-2(\gamma_d+\gamma_s)a}\right.\right.$$
$$\left.\left. + 8\gamma_s\gamma_d(\gamma_s^2 + \xi^2)(\gamma_2 + 3\xi^2)\mathrm{e}^{-(\gamma_d+\gamma_s)a}\right)\right], \tag{C.7}$$

$$\mu a_{22} = -\gamma_s \frac{p^2}{c_s^2}\left[\frac{1}{R} + \frac{1}{\mathscr{K}}\left(S - s\mathrm{e}^{-2\gamma_d a} + (S + 8\xi^2\gamma_s\gamma_d)\mathrm{e}^{-2\gamma_s a} - (s - 8\xi^2\gamma_s\gamma_d)\mathrm{e}^{-2(\gamma_d+\gamma_s)a}\right)\right]; \tag{C.8}$$

we have introduced $q_1 = (\xi^2 + \gamma_s^2 + 2\gamma_s\gamma_d)$ and $q_2 = (\xi^2 + \gamma_s^2 - 2\gamma_s\gamma_d)$ for convenience.

The leading exponential terms required in the text and relevant to the present article are given by a Taylor's expansion. They are intricately connected with the reflection and transmission coefficients but this is, often, not transparent when each component is taken in turn:

$$\mu R a_{11} \sim -\gamma_d \frac{p^2}{c_s^2}\left\{2 + \frac{s}{S}\left(1 + \frac{r}{R}\right)\mathrm{e}^{-2\gamma_d a} - \frac{S + 8\xi^2\gamma_s\gamma_d}{S}\left(1 - \frac{r}{R}\right)\mathrm{e}^{-2\gamma_s a} + 2\left(1 + \frac{s}{S}\right)\left(1 - \frac{r}{R}\right)\mathrm{e}^{-(\gamma_d+\gamma_s)a}\right.$$
$$\left. + \frac{s^2 r}{S^2 R}\left(1 + \frac{r}{R}\right)\mathrm{e}^{-4\gamma_d a} - \frac{(S + 8\xi^2\gamma_s\gamma_d)^2 r}{S^2 R}\left(1 - \frac{r}{R}\right)\mathrm{e}^{-4\gamma_s a}\right\}, \tag{C.9}$$

$$\mu R^2 a_{12} = -\mu R^2 a_{21}$$
$$\sim 4\mathrm{i}\xi\gamma_s\gamma_d(\xi^2 + \gamma_s^2)\frac{p^2}{c_s^2}\left[\frac{s}{S}\mathrm{e}^{-2\gamma_d a} + \frac{S + 8\xi^2\gamma_s\gamma_d}{S}\mathrm{e}^{-2\gamma_s a} - \frac{s + S + 8\xi^2\gamma_s\gamma_d}{S}\mathrm{e}^{-(\gamma_d+\gamma_s)a} + \frac{s^2 r}{S^2 R}\mathrm{e}^{-4\gamma_d a}\right.$$
$$\left. + \frac{(S + 8\xi^2\gamma_s\gamma_d)^2 r}{S^2 R}\mathrm{e}^{-4\gamma_s a}\right], \tag{C.10}$$

$$\mu R a_{22} \sim -\gamma_s \frac{p^2}{c_s^2}\left\{2 - \frac{s}{S}\left(1 - \frac{r}{R}\right)\mathrm{e}^{-2\gamma_d a} + \frac{S + 8\xi^2\gamma_s\gamma_d}{S}\left(1 + \frac{r}{R}\right)\mathrm{e}^{-2\gamma_s a} + 2\left(1 + \frac{s}{S}\right)\left(1 - \frac{r}{R}\right)\mathrm{e}^{-(\gamma_d+\gamma_s)a}\right.$$
$$\left. - \frac{s^2 r}{S^2 R}\left(1 - \frac{r}{R}\right)\mathrm{e}^{-4\gamma_d a} + \frac{(S + 8\xi^2\gamma_s\gamma_s)^2 r}{S^2 R}\left(1 + \frac{r}{R}\right)\mathrm{e}^{-4\gamma_s a}\right\}. \tag{C.11}$$

Similarly, the expressions for the stresses and displacements are recovered from an expansion in terms of the displacement potentials.

References

Achenbach, J.D., 1973. Wave Propagation in Elastic Solids. North-Holland, Amsterdam.

Atkinson, C., 1975. Some results on crack propagation in media with spatially varying elastic moduli. International Journal of Fracture 21, 619–628.

Atkinson, C., 1977. On quasi-static problems of cracks in a non-homogeneous elastic layer. Acta Mechanica 26, 103–113.

Atkinson, C., Craster, R.V., 1992a. The application of invariant integrals in diffusive elastic solids. Philosophical Transactions of the Royal Society of London A 339, 231–263.

Atkinson, C., Craster, R.V., 1992b. Fracture in fully coupled dynamic thermoelasticity. Journal of the Mechanics and Physics of Solids 40, 1415–1432.

Atkinson, C., Craster, R.V., 1995a. Invariant integrals, stress concentrations and energy release rates. In: Cherepanov, C. (Ed.), Fracture: A Topical Encyclopedia of Current Knowledge Dedicated to Alan Arnold Griffith. Krieger, New York, pp. 496–517.

Atkinson, C., Craster, R.V., 1995b. Theoretical aspects of fracture mechanics. Progress in Aerospace Sciences 31, 1–83.
Bueckner, H.F., 1970. A novel principle for the computation of stress intensity factors. Journal of Applied Mathematics and Mechanics (ZAMM) 50, 529–546.
Choi, H.J., 1997. A periodic array of cracks in a functionally graded nonhomogeneous medium loaded under in-plane normal and shear. International Journal of Fracture 88, 107–128.
Craster, R.V., Atkinson, C., 1994. Mixed boundary value problems for non-homogeneous elastic materials. Quarterly Journal of Mechanics and Applied Mathematics 47, 183–206.
de Hoop, A.T., 1960. A modification of Cagniard's method for solving seismic pulse problems. Applied Scientific Research B 8, 349–356.
Ergüven, M.E., Gross, D., 1999. On the penny-shaped crack in inhomogeneous elastic materials under normal extension. International Journal of Solids and Structures 36, 1869–1882.
Eshelby, J.D., 1951. The force on an elastic singularity. Philosophical Transactions of the Royal Society of London A 244, 87–112.
Eshelby, J.D., 1970. Energy relations and the energy-momentum tensor in continuum mechanics. In: Kanninen, M.F., et al. (Eds.), Inelastic Behaviour of Solids. McGraw-Hill, New York, pp. 77–115.
Flinn, E.A., Dix, C.H., 1962. Reflection and Refraction of Progressive Seismic waves. McGraw-Hill, New York (L. Cagniard, Trans.; Reflection et refraction des ondes seismique progressives. Gauthiers-Villars, Paris, 1939).
Freund, L.B., 1990. Dynamic Fracture Mechanics. Cambridge University Press, Cambridge, MA.
Garvin, W.W., 1956. Exact transient solution of the buried line source problem. Proceedings of the Royal Society of London A 234, 528–541.
Gradshteyn, I.S., Ryzhik I.M., 1980. Table of Integrals, Series and Products, Academic Press, London (Corrected and enlarged edition).
Haak, K.F.I., Kooij, B.J., 1996. Transient acoustic diffraction in a fluid layer. Wave Motion 23, 139–164.
Harris, J.G., 1980. Diffraction of a crack by a cylindrical longitudinal pulse. Journal of Applied Mathematics and Physics (ZAMP) 31, 367–381.
Kooij, B.J., Quak, D., 1988. Three-dimensional scattering of impulsive acoustic waves by a semi-infinite crack in the plane interface of a half-space and a layer. Journal of Mathematical Physics 29, 1712–1721.
Miklowitz, J., 1978. The Theory of Elastic Waves and Waveguides. North-Holland, Amsterdam.
Nilsson, F., 1973. A path-independent integral for transient crack problems. International Journal of Solids and Structures 9, 1107–1115.
Noble, B., 1958. Methods Based on the Wiener–Hopf Technique. Pergamon Press, New York.
Rice, J.R., 1968. A path independent integral and the approximate analysis of strain concentration by notches and cracks. Journal of Applied Mechanics 35, 379–386.
Thau, A., Lu, T.H., 1971. Transient stress intensity factors for a finite crack in an elastic solid caused by a dilatational wave. International Journal of Solids and Structures 7, 731–750.
Tsai, C.H., Ma, C.C., 1992. Transient analysis of a semi-infinite crack subjected to dynamic concentrated forces. Journal of Applied Mechanics 59, 804–811.
Tsai, C.H., Ma, C.C., 1993. The stress intensity factor of a subsurface inclined crack subjected to dynamic impact loading. International Journal of Solids and Structures 30, 2163–2175.
Tsai, C.H., Ma, C.C., 1997. Theoretical transient analysis of the interaction between a dynamically propagating in-plane crack and traction-free boundaries. Journal of Applied Mechanics 64, 819–827.